1965

A photoelastic study of the effect of certain geometric variables on the plane stress distribution in an electrical insulator body

Richard L. Pendleton

A PHOTOELASTIC STUDY OF THE EFFECT OF CERTAIN GEOMETRIC VARIABLES ON THE PLANE STRESS DISTRIBUTION IN AN ELECTRICAL INSULATOR BODY

by

Richard L. Pendleton

A

THESIS

submitted to the faculty of the

UNIVERSITY OF MISSOURI AT ROLLA

in partial fulfillment of the requirements for the

Degree of

MASTER OF SCIENCE IN MECHANICAL ENGINEERING

Rolla, Missouri

1965

Approved by

Peter Hansen (Advisor)

M. G. Parry

H. D Pyron

Lyman L. Francis

ABSTRACT

Photoelastic models were used to indicate stress patterns in various geometrically designed shapes. Each model represented a two-dimensional cross-section of the interior portion of an axially symmetrical porcelain electrical insulator. Five different loading pins were combined with three loading heads to produce eleven models. The maximum stress in each model was determined using a photoelastic method of stress analysis. An attempt was made to select the best structural design to be used in an electrical insulator. The test results indicate that the most desirable stress distribution is obtained using a single step loading pin and that the loading head angle and loading pin angle should be approximately equal to twenty-five degrees measured from the vertical plane.

ACKNOWLEDGEMENTS

The author wishes to express his sincere appreciation to Dr. P. G. Hansen, Professor of Mechanics, University of Missouri at Rolla, for his guidance and helpful advice throughout this investigation. Gratitude is also due Dr. D. E. Day, Professor of Ceramic Engineering, University of Missouri at Rolla, for his advice and suggestions concerning many phases of this study.

The assistance of the A. B. Chance Company in the form of supplies, materials, and information was invaluable to the investigator.

The author wishes to thank Mr. E. A. Moss for his able technical assistance in preparing the models and collecting data.

A special note of appreciation is due my wife, Lavon, for her constant support and assistance.

TABLE OF CONTENTS

LIST OF FIGURES v

LIST OF TABLES. vii

LIST OF SYMBOLS viii

I. STATEMENT OF THE PROBLEM. 1

II. REVIEW OF LITERATURE. 9

III. PREPARATION OF THE MODEL. 11

IV. BASIC THEORY AND EXPERIMENTAL PROCEDURE 16

V. SUMMARY OF RESULTS. 32

APPENDICES. 36

APPENDIX A 37

APPENDIX B 46

BIBLIOGRAPHY. 58

VITA. 59

LIST OF FIGURES

1. Photograph of One-Half of an Insulator 2
2. Drawing of Insulator 3
3. Cross-Section of Loading Head Showing Head Angle . . 5
4. Types of Model Loading Pins. 6
5. Diagram for Relating X and Z 8
6. Pictorial Drawing of Model Loading Head and Loading Pin. 12
7. Fringe Patterns for Standard-Step and Parabolic Models 20
8. Isoclinic Patterns for Standard-Step and Parabolic Models 21
9. Fringe Patterns for Minus-Step and Plus-Step Models. 22
10. Isoclinic Patterns for Minus-Step and Plus-Step Models 23
11. Fringe Patterns for Standard Two-Step and Plus Two-Step Models 24
12. Isoclinic Patterns for Standard Two-Step and Plus Two-Step Models 25
13. Fringe Patterns for Minus Parabolic and Plus Parabolic Models. 26
14. Isoclinic Patterns for Minus Parabolic and Plus Parabolic Models. 27
15. Fringe Patterns for Plus-Plus Step and Minus-Minus Step Models. 28
16. Isoclinic Patterns for Plus-Plus Step and Minus-Minus Step Models. 29
17. Fringe Pattern for Minus Two-Step Model. 30
18. Isoclinic Pattern for Minus Two-Step Model 31
19. Stress Distribution on a Differential Element. 37

LIST OF FIGURES (Cont.)

20. Drawing of a General Model Cross-Section Showing Rectangular Segments Used in the Calculations . . . 39

21. Free Body Diagram of a Rectangular Element Extracted from a Model. 40

22. Graph of Shearing Stress Versus Displacement on the X Axis 43

LIST OF TABLES

I. Symbols and General Description for All Models Tested 19

II. Principal Stresses and Maximum Shearing Stress for All Models Tested. 34

III. Shearing Stress Calculations. 41

IV. Principal Stress Calculations 44

V. Principal Stress and Maximum Shearing Stress for Minus-Minus Step Model. 47

VI. Principal Stress and Maximum Shearing Stress for Plus Plus-Step Model. 48

VII. Principal Stress and Maximum Shearing Stress for Standard-Step Model 49

VIII. Principal Stress and Maximum Shearing Stress for Minus-Step Model. 50

IX. Principal Stress and Maximum Shearing Stress for Plus-Step Model 51

X. Principal Stress and Maximum Shearing Stress for Standard-Parabolic Model. 52

XI. Principal Stress and Maximum Shearing Stress for Minus-Parabolic Model 53

XII. Principal Stress and Maximum Shearing Stress for Plus-Parabolic Model. 54

XIII. Principal Stress and Maximum Shearing Stress for Standard Two-Step Model 55

XIV. Principal Stress and Maximum Shearing Stress for Minus Two-Step Model. 56

XV. Principal Stress and Maximum Shearing Stress for Plus Two-Step Model 57

LIST OF SYMBOLS

A	axis parallel to X axis
C	axis parallel to X axis
F	model fringe value
h	total length of the X axis
N	fringe order at a point
p	algebraic maximum normal stress
q	algebraic minimum normal stress
R	radius of a horizontal cross-section of an unloaded insulator
X	rectangular coordinate axis and position coordinate
Y	rectangular coordinate axis and position coordinate
Z	rectangular coordinate axis and position coordinate
$\frac{x}{h}$	ratio of position on the X axis to the total length of the X axis
ΔX	finite increment of length on the X axis
ΔY	finite increment of length on the Y axis
δ_R	radial deformation of a horizontal cross-section of a loaded insulator
δ_x	deformation of a horizontal cross-section of a loaded insulator in the X direction
δ_z	deformation of a horizontal cross-section of a loaded insulator in the Z direction
θ	arbitrary angle
θ_p	angle from a horizontal axis to the plane of the algebraic maximum stress (p)
θ_q	angle from a horizontal axis to the plane of the algebraic minimum stress (q)
θ_T	angle from a horizontal axis to the plane of maximum shearing stress (τ_{max})
ϕ	angle from a horizontal axis to an arbitrary X axis

LIST OF SYMBOLS (Cont.)

σ_C	stress normal to the C axis
σ_A	stress normal to the A axis
σ_{x_N}	normal stress in the X direction at point N in the model
σ_{y_N}	normal stress in the Y direction at point N in the model
σ_z	normal stress in the Z direction
τ_{xy}	shearing stress acting on the X Y planes
τ_{xy_0}	shearing stress on a plane normal to the X axis in the Y direction at point O
τ_{xy_1}	shearing stress on a plane normal to the X axis in the Y direction at point 1
τ_{yC}	shearing stress on a plane normal to the Y axis in the C direction
τ_{yA}	shearing stress on a plane normal to the Y axis in the A direction
τ_{max}	maximum shearing stress

I. STATEMENT OF THE PROBLEM

An axially symmetrical electrical insulator of the type shown in Figures 1 and 2 is required to withstand a centric load through a vertical axis of symmetry. The insulators may be used singly or in stacked combinations with the pin of each insulator connected to the head of the next insulator. The insulator is basically composed of a head, porcelain body, pin, and portland cement. The loading head is normally made of steel and gives structural rigidity to the system. The head is connected by a yoke to another insulator or to the power line pole by a yoke. The steel loading pin is inserted into the porcelain body and is connected through a yoke to a high voltage power line or to another insulator. The inserted portion of the pin should be designed such that the pin will neither slip out of the porcelain nor induce an undesirable stress distribution within the pin or the porcelain body. The main body of the insulator is made of porcelain and is the primary insulating medium. The portion of the porcelain within the head is subjected to large stresses and consequently must have mechanical strength as well as insulating properties. The portion of the porcelain outside the head, called the skirt, carries virtually no mechanical load and is present primarily to prevent arcing around the insulator body. The pin and head are bonded to the porcelain using neat Portland cement.

This is a study of the influence of pin design and head design on the stress distribution in the porcelain body.

Figure 1. Photograph of One-Half of an Insulator.

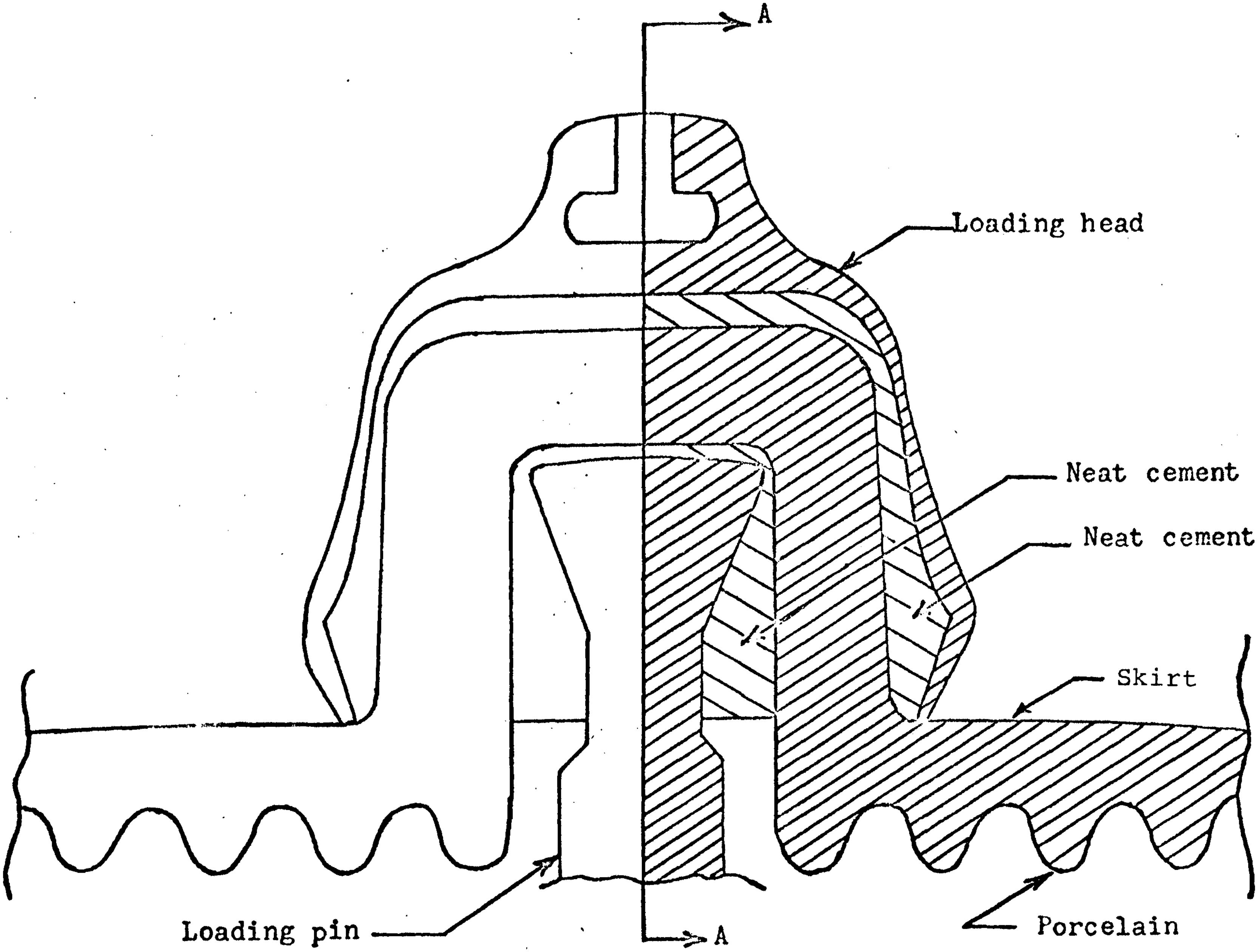

Figure 2. Drawing of Insulator

Three basic head designs were used by varying the head angle. (Figure 3). Head angles of 17 1/2°, 22 1/2°, and 27 1/2° were used. Five pin designs were used. (See Figure 4). Three single step pins with pin angles of 17 1/2°, 22 1/2°, and 27 1/2° were used as well as a two-step pin and a parabolic pin. These five pins combined with the three head designs were used to construct eleven models. Due to the nature of the structure it was decided to construct a transparent model of the structure and to use the photoelastic method to determine the induced stress distribution. The models were made to represent the porcelain and cement as a homogeneous and isotropic fill between the head and pin.

It is the opinion of the investigator that the bond between the cement and the head and between the cement and the pin fails at a relatively small load but that the bond between the cement and the porcelain is maintained until fracture. This opinion is based on examination of insulators loaded to failure. If this is true there must exist a continuity of strain between the cement and porcelain until failure of the structure. The neglected non-homogeneity would certainly have relevance to the exact magnitude of the stress involved but was assumed to have a negligible effect on the resultant strains. The eleven models were evaluated on a comparative basis for the purpose of selecting the best design and it was assumed that the neglected non-homogeneity would have virtually the same effect on all of the models.

The problem under consideration is primarily a compara-

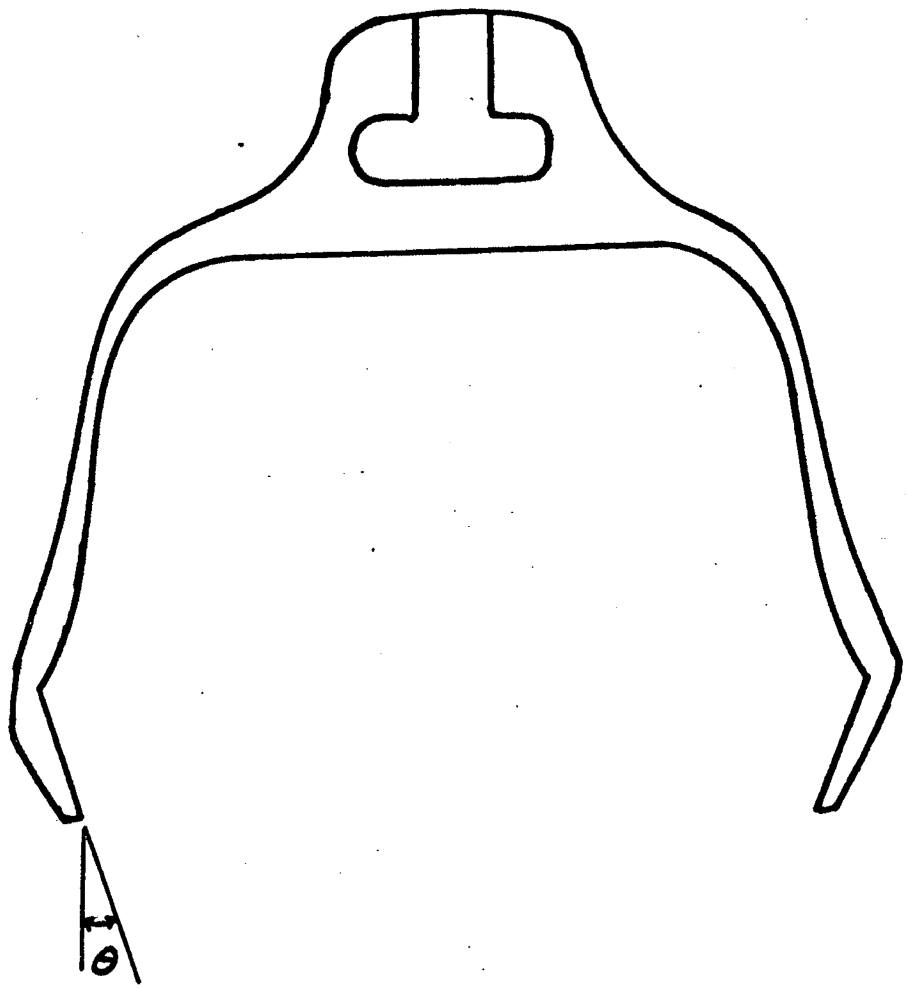

Figure 3. Cross-Section of Loading Head Showing Head Angle

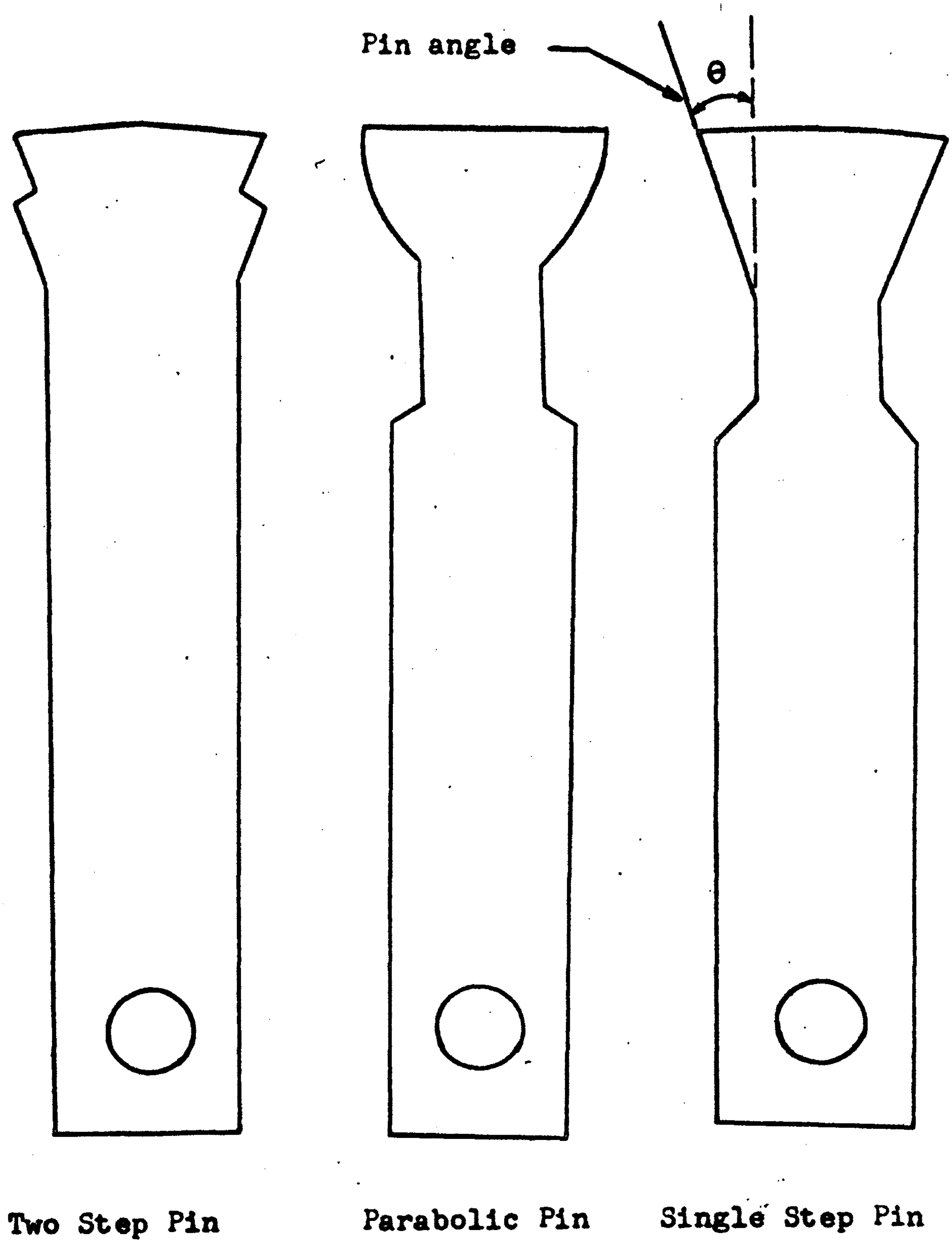

Figure 4. Types of Model Loading Pins

tive study of the effect of varying the head angle and pin design on the distribution of strains and stresses within the porcelain and cement portion of the insulator. The actual insulator is in a triaxial state of stress under normal load conditions. It is possible to show that the magnitude of stresses obtained using a thin model in a biaxial state of stress is directly proportional to the magnitude of stress that would be obtained using a three dimensional model in a triaxial state of stress. Consider one quadrant of a horizontal cross-section of the insulator (See Figure 5). Because of the symmetry of both the load and geometry about the vertical centroidal axis, Y, the radial deformation of the body must be independant of the angle θ measured from the Z axis in the X-Z plane. The cross-section is a circle of radius R prior to loading. After the load is applied the section remains circular but with a radius of $R + \delta R$. The horizontal cross section is considered to be in the X-Z plane. From Figure 5 the following relationship was obtained:

$$Z = 2(R+\delta R)\ \mathrm{Cos}(\theta-\delta\theta) - 2R\mathrm{Cos}\theta.$$

For any arbitrary angle θ it can be seen that $\delta\theta$ is a function of δZ only and the variable δZ is directly proportional to δR and δX for any angle θ and any height Y. The preceding analysis is valid for all designs tested, consequently, even though the magnitude of the stresses obtained in a plane stress model will be in considerable error the deletion of σ_z introduces a proportionate error in all of the models and a comparative analysis of the various models will be valid.

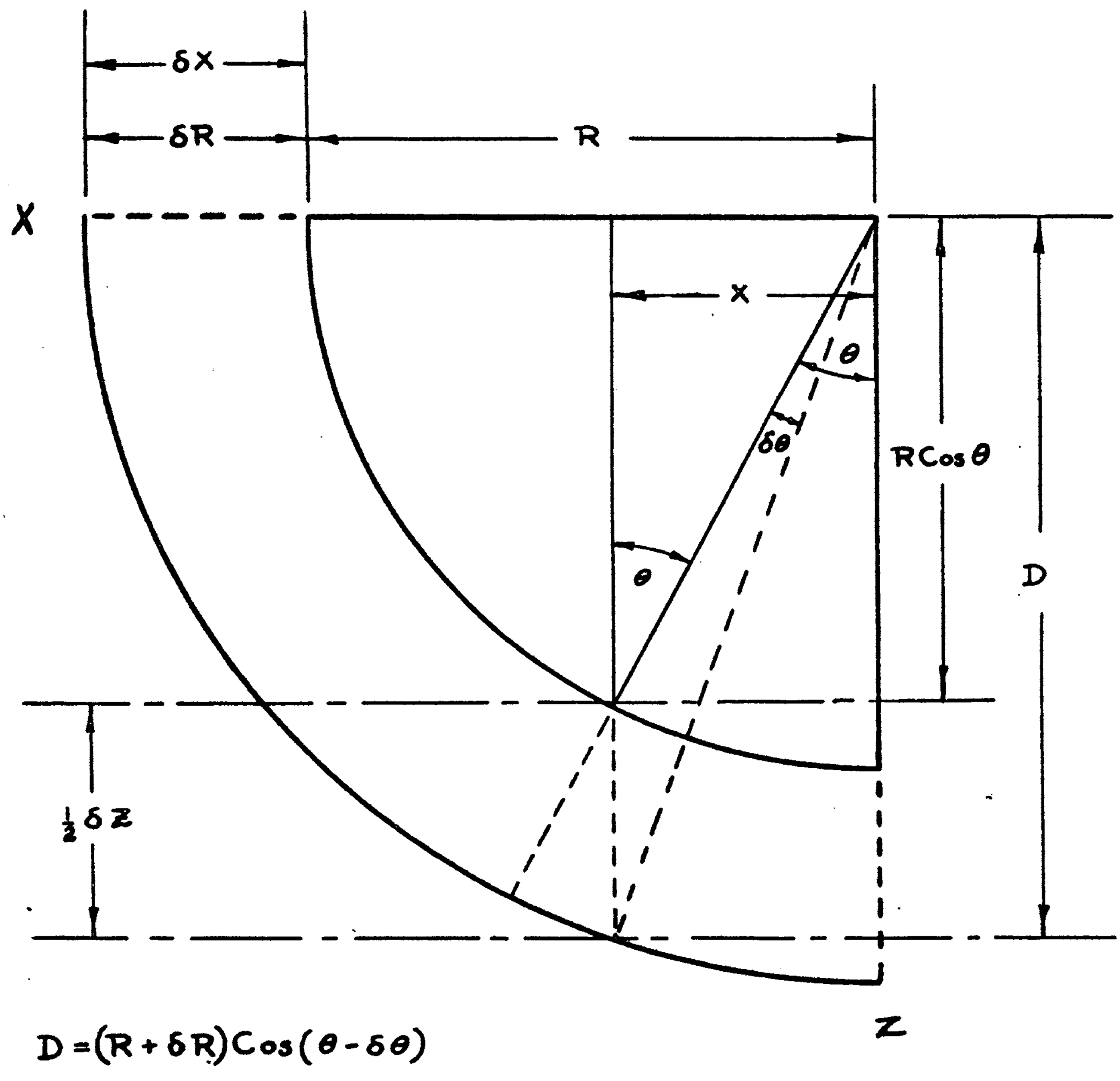

Figure 5. Diagram for Relating X and Z

II. REVIEW OF LITERATURE

No literature directly related to the problem under consideration was found.

Formable epoxy resins are quite commonly used by experimenters using the photoelastic method. R. D. Cook[1] used a combination of two parts by weight Araldite of 6020 and one part by weight of Phthalic anhydride, prepared at room temperature, to cast cylinders. These cylinders exhibited a type of mottling, apparently due to the thickness of the casting, which was alleviated by heat treating. A similar type of mottling was observed during the present investigation which was reduced both by reducing the thickness of the model and by heat treatment. Araldite 6020 is similar in composition to Araldite 6010.

The shear difference method of calculating normal stresses using data obtained with a standard crossed bench type polariscope is described by M. M. Frocht[2]. J. J. Polivka and H. D. Eberhart[3] describe a method for calculating principal stresses using photoelastic fringe data and photoelastic isoclinic data. This investigator used the shear difference method to calculate the normal stress along one axis and the method of Polivka and Eberhart to obtain the remaining desired normal stresses.

An analytical solution to the problem under consideration would be virtually impossible to solve because of the large, varying thickness, unknown distribution of the load between the head and the body of the insulator, and the irregularity of the geometry of the structure.

III. PREPARATION OF THE MODEL

The photoelastic study using a bench-type polariscope required a transparent birefringent model. Loading heads and loading pins were used that could be considered rigid as compared to the model. Six inch by six inch steel plates one-half inch thick were used to construct the loading heads. The interior contour of a diametrical cross-section of each of the steel insulator heads was cut out of the steel plates. (See Figure 6). The exterior contour of a diametrical cross-section of each of the pins was cut from one-half inch thick flat steel plate to form the loading pins.

An attempt was made to machine models from the commercial photoelastic material CR-39 that would exactly fit the loading head and pin. The method of machining of CR-39 was of no practical value because of minor ridges that existed on the steel loading parts which were impossible to machine into the model. The ridges created stresses in the model with no external load applied to the mechanism as well as stress concentrations in the model when an external load was applied.

It was decided to cast a formable epoxy resin into the loading head with the loading pin positioned properly. When the epoxy model solidified it would have the exact contour of the loading head and pin with no stress concentrations because of improper fit between the model and loading mechanism. An epoxy resin consisting of 50% by weight of Araldite 6010 and 50% by weight of Versimid 140 was found to

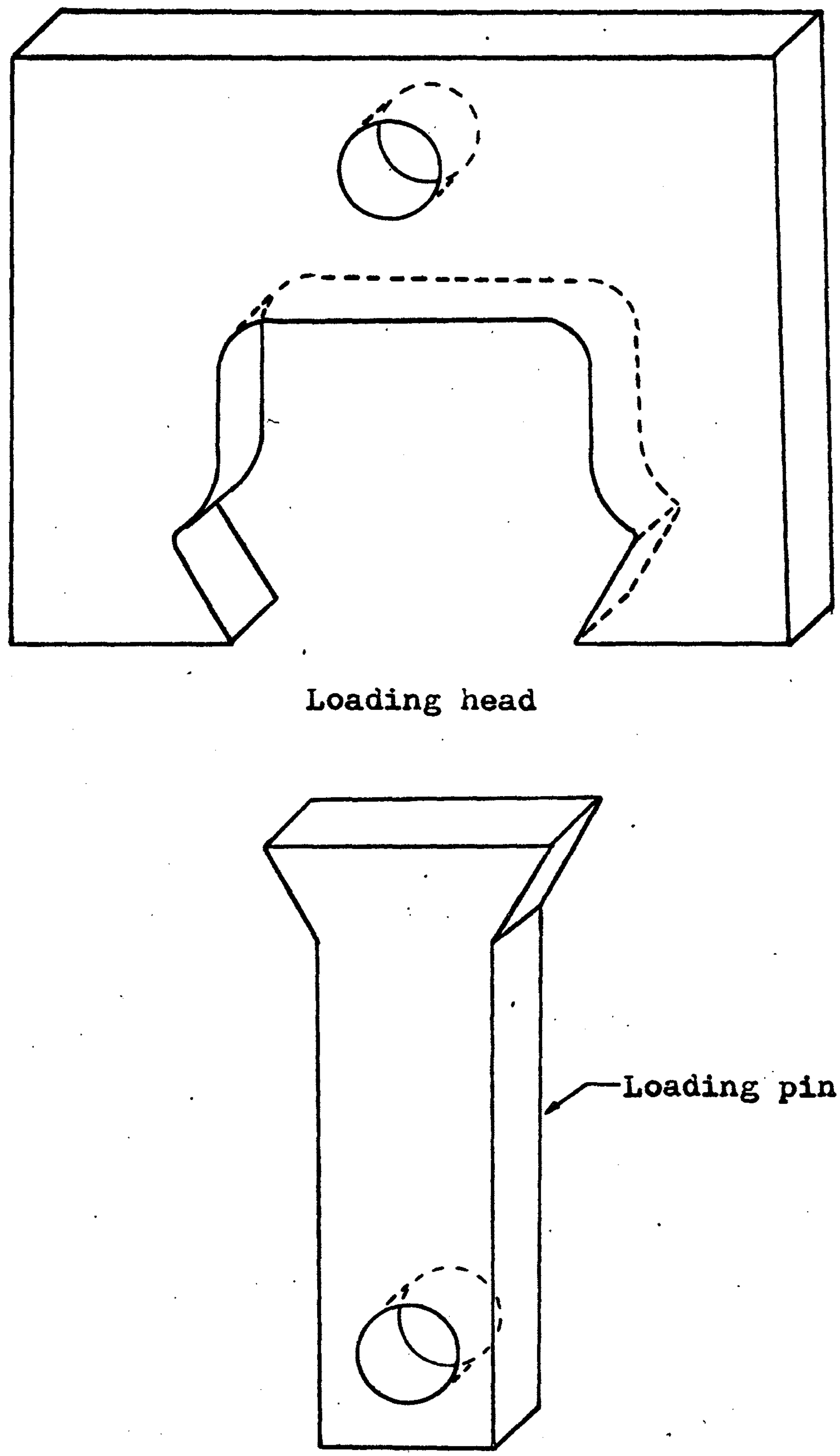

Figure 6. Pictorial Drawing of Model Loading Head and Loading Pin

possess the properties required for this purpose. The resin cured completely enough at room temperature to be tested within two weeks with no retention of initial internal stresses. Curing was accelerated using a heat treatment which allowed the model to be tested within three days.

It was found necessary to make the models one-fourth inch thick. A one-half inch thick model was undesirably insensitive to load and also created curing problems exhibited by initial fringes. These problems were alleviated by using a one-fourth inch thick model. Two one-eighth inch thick spacers were machined for each model that was made. These spacers had the approximate shape of the finished model. The loading pin was properly positioned and the spacers placed in the head-pin combination so that a one-fourth inch thick void with the exact shape of the desired model existed. The two spacers were on opposite sides of this void. This mold was coated with polyvinyl alcohol which acted as a mold release agent. The mold was then sealed using polyethylene tape. The Araldite and Versimid were thoroughly mixed, placed in a vacuum to remove the entrained air, and poured into the mold. The resin was heated to 375°F. for approximately one hour. The temperature was reduced step-wise at a rate of twenty degrees per hour until it had been reduced to room temperature. Cure was completed at room temperature. The model was removed from the mold after approximately twenty-four hours and allowed to cure for an additional forty-eight hours before testing. The finished model exhibited some shadows due to initial internal stresses but there were no fringes visible when it was placed in the polariscope.

No precise tests were conducted to determine the creep characteristics of the models but the fringe pattern obtained under load did not vary sufficiently to be discernible during a time interval of fifteen minutes. When the load was removed the resin returned to a normal clear image almost instantaneously.

The appearance of the fringe pattern and isoclinic pattern was sharp and distinct. If the load was removed and then replaced, the same image of fringes or isoclinics was obtainable with no visible variation in the stress concentrations or general pattern.

The modulus of elasticity and Poisson's ratio were not obtained for the resin because they were not pertinent to the calculations. The material fringe value was obtained by casting a rectangular slab for each batch of resin that was mixed to cast the models. The rectangles were machined to a specified width and had a constant thickness so that the cross-sectional area was known. The rectangle was loaded gradually in tension and the load was recorded each time a fringe appeared. The axial stress was calculated for the rectangle at the relevant loads, and a graph of stress versus fringe order was plotted. The slope of this straight line is the model fringe value in psi/fringe. The material fringe value was calculated as the product of the model fringe value and the model thickness.

The model fringe value was used to convert the units of the calculated stresses from fringes to pounds per square inch.

IV. BASIC THEORY AND EXPERIMENTAL PROCEDURE

The model was placed in a bench-type polariscope and a load of one hundred and eighty pounds was applied. A fringe pattern for each model tested was obtained using monochromatic light and a standard crossed polariscope. The fringe patterns were photographed and all fringe data were obtained from the photographs. The isoclinics were obtained using a white light source with the quarter wave plates removed from the standard crossed polariscope arrangement. The polarizer and analyzer remained crossed. An image of the model was projected on a screen and isoclinic parameters from zero degrees to ninety degrees in ten degree increments were superimposed on a tracing made of the projected image. The isoclinic parameters were corrected to agree with known boundary conditions and adjusted to follow parameter patterns to which they must theoretically adhere.(2)

The fringe order at any point is proportional to the maximum shearing stress at that point. If N is the fringe order at a point and F is the model fringe value then the maximum shearing stress at that point is (N) (F). An isoclinic is a locus of points that have a constant inclination of principal stress. The isoclinics were measured from a horizontal axis and the parameter of the isoclinic at any point represents the angle to the plane on which a principal stress acts as measured from the horizontal. Let ϕ be the angle from the plane of principal stress to any arbitrary X axis. The shearing stress on that axis can be shown to be (N) (F) Sin 2θ. From the experimental data obtained the factors N and Sin 2θ could be found for all points on the model and consequently the shearing stress at any point in the model and along any desired axis could be calculated.

The maximum stress in the model was considered to be the primary basis of comparison upon which to evaluate the relative stress bearing efficacy of the geometrically varied models. It was assumed that the point of maximum stress would occur at or near the point of highest fringe order in the model. The shear difference method was used to determine the normal stresses and the shear stress on two perpendicular planes.[2] The basic theory of stresses at a point could then be used to determine the principal stresses at any point in the model. Principal stresses were calculated at eleven points equally spaced from a point of zero stress to the point of maximum fringe order. A more detailed explanation of the calculating procedures can be found in the sample calculations. (See Appendix A).

Eleven models were constructed and tested. Calculations were made on all of the models even though some of the models showed stress concentrations of much greater fringe order than the others. The basic head design used was the Lancaster Standard head. (See Figure 3). The Lancaster Standard head normally has a lip angle of 22 1/2° measured from the vertical. The only geometric variation of the head during these tests was in the magnitude of the lip angle. Those models labeled Plus had a lip angle of 27 1/2° and those labeled Minus were constructed with an angle of 17 1/2°. Three basic pin designs were used during these tests. Both the Two Step and the Parabolic pins were tested in combination with all three head variations. The Single Step pin normally is constructed with the oblique edges making an angle of 22 1/2° with the vertical. This pin, called the Step pin, was also tested with all three head variations. The Plus pin, with an angle of 27 1/2°, was tested only with the Plus head and the Minus pin, with an angle of 17 1/2°, was tested only with the Minus head.

It was hoped that the combinations would indicate the relative effectiveness of pin design in reducing the maximum stress within the model and also indicate trends for obtaining the optimum angle or combination of angles for the head and pin. The nomenclature for each model with the respective head angle and pin type is given in Table I. The fringe pattern in the models with a load of one hundred and eighty pounds is shown in Figures 6, 8, 10, 12, 14, and 16. The isoclinic parameters from 0° to 90° in 10° increments for a load of one hundred and eighty pounds is shown in Figures 7, 9, 11, 13, 15, and 17. For each model the isoclinic parameters are on the page immediately following the fringe pattern.

TABLE I. Symbols and General Description for All Models Tested

MODEL SYMBOL	TYPE OF HEAD	HEAD ANGLE	PIN TYPE AND PIN ANGLE
Std.-Step	Lancaster Standard	22 1/2°	Single Step 22 1/2°
Plus-Plus Step	Lancaster Standard	27 1/2°	Single Step 27 1/2°
Minus-Minus Step	Lancaster Standard	17 1/2°	Single Step 17 1/2°
Plus-Step	Lancaster Standard	27 1/2°	Single Step 22 1/2°
Minus-Step	Lancaster Standard	17 1/2°	Single Step 22 1/2°
Std.-Parabolic	Lancaster Standard	22 1/2°	Parabolic
Std.-Two Step	Lancaster Standard	22 1/2°	Two Step
Plus-Parabolic	Lancaster Standard	27 1/2°	Parabolic
Plus-Two Step	Lancaster Standard	27 1/2°	Two Step
Minus-Parabolic	Lancaster Standard	17 1/2°	Parabolic
Minus-Two Step	Lancaster Standard	17 1/2°	Two Step

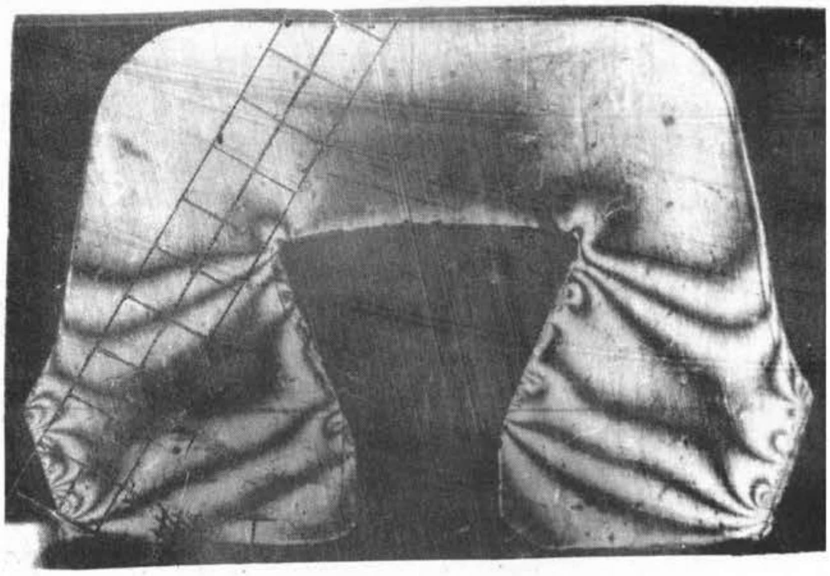

Standard-Step Model.

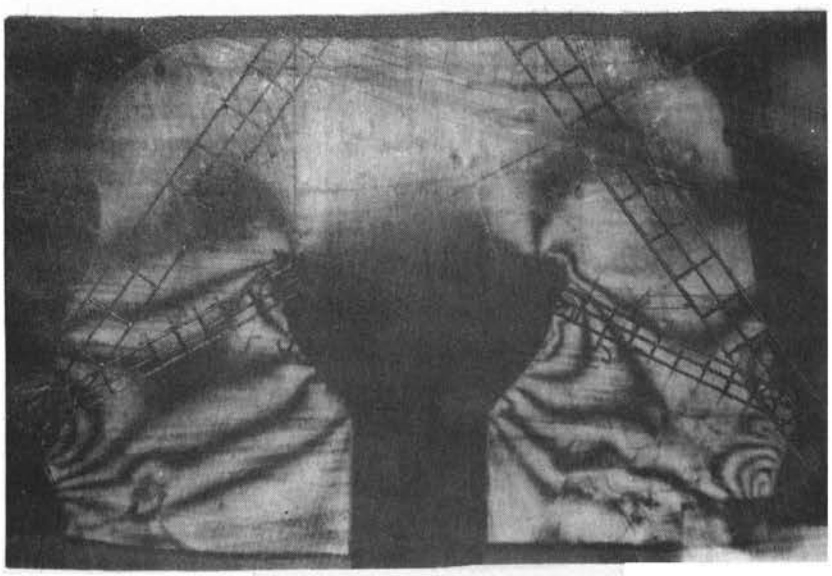

Parabolic Model.

Figure 7. Fringe Patterns for Standard-Step and Parabolic Models.

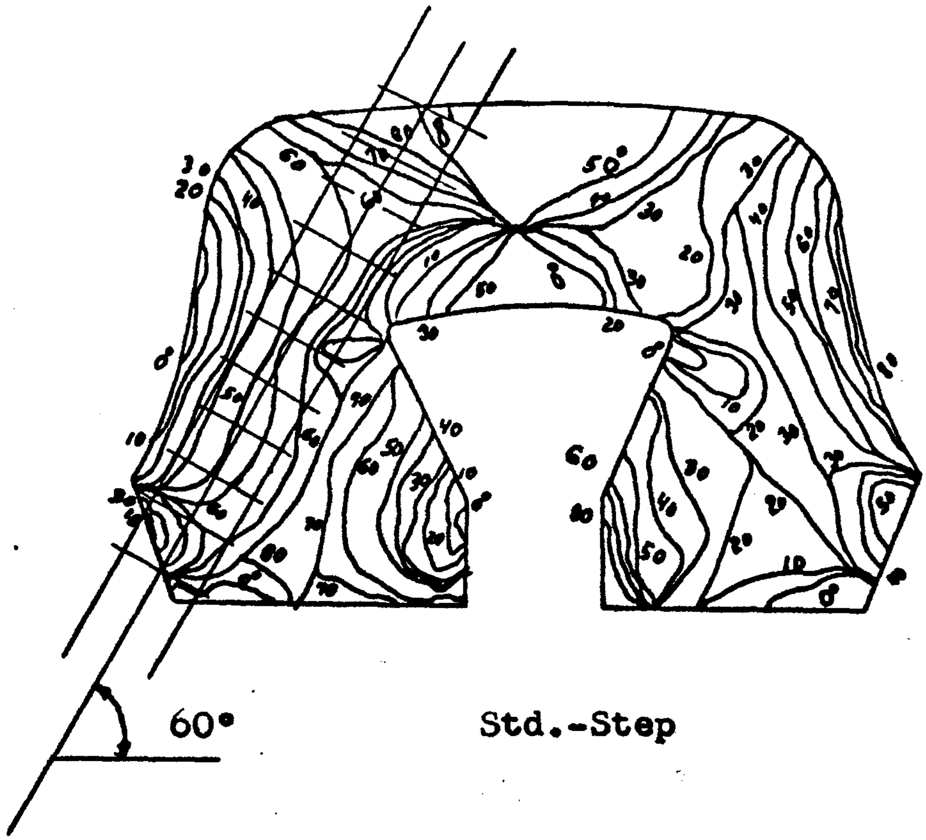

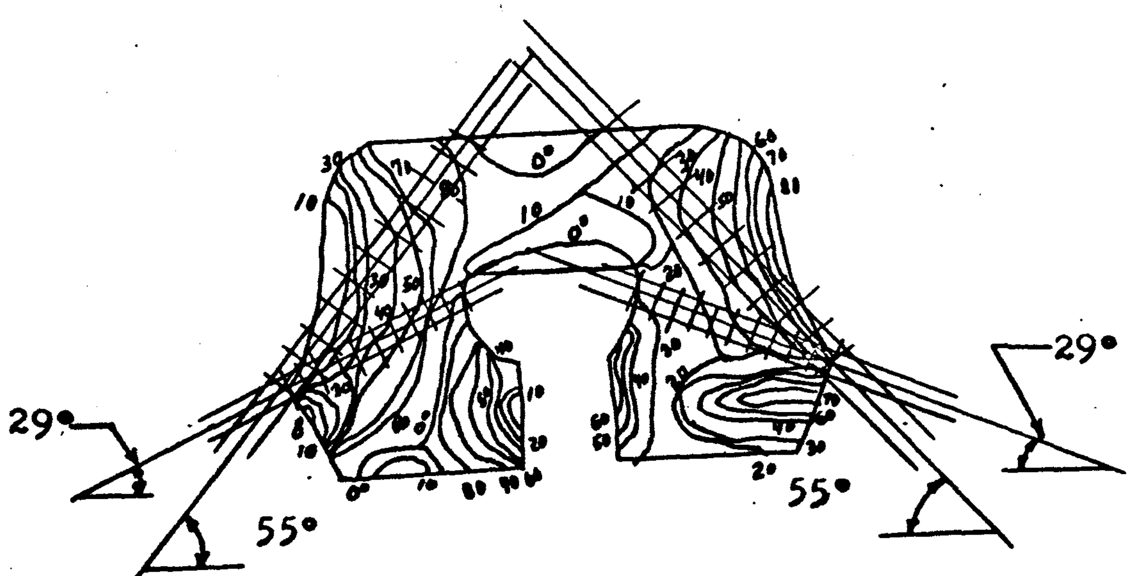

Figure 8. Isoclinic Patterns for Standard-Step and Parabolic Models

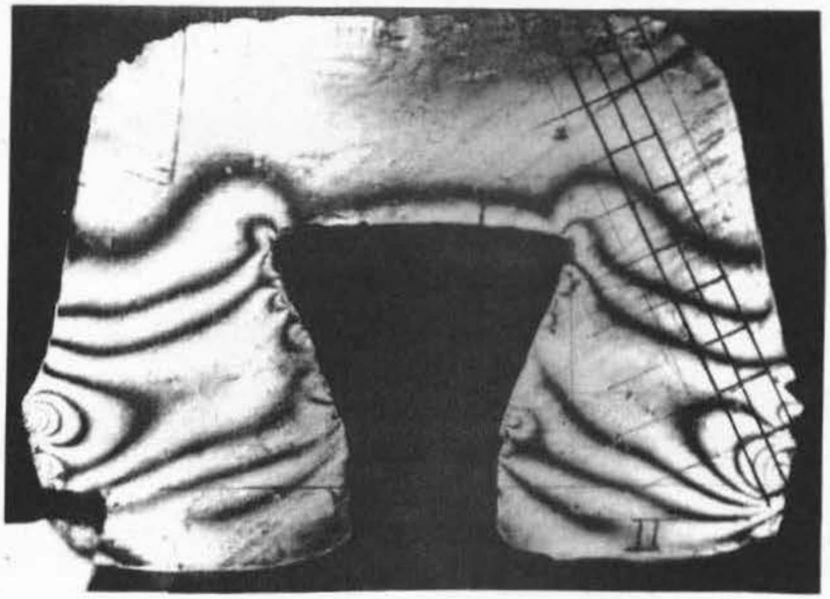

Minus-Step Model.

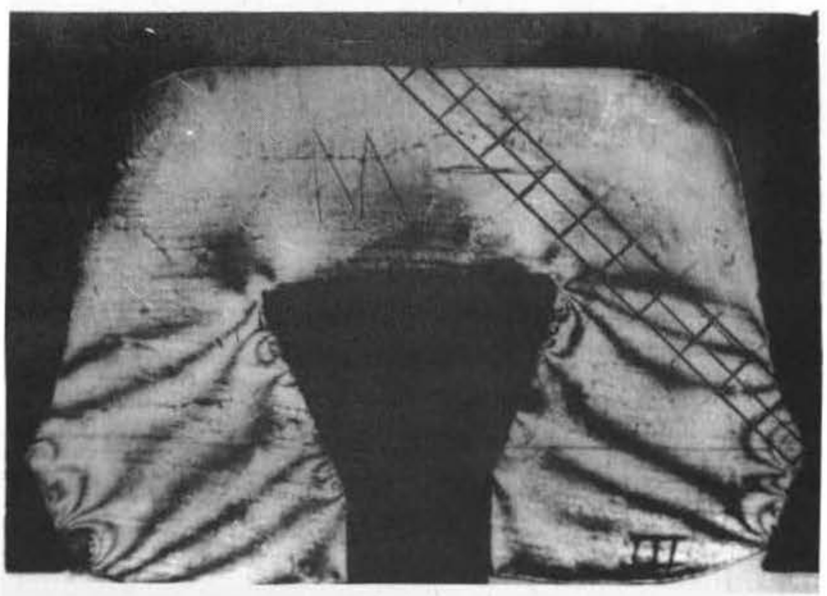

Plus-Step Model.

Figure 9. Fringe Patterns for Minus-Step and Plus-Step Models.

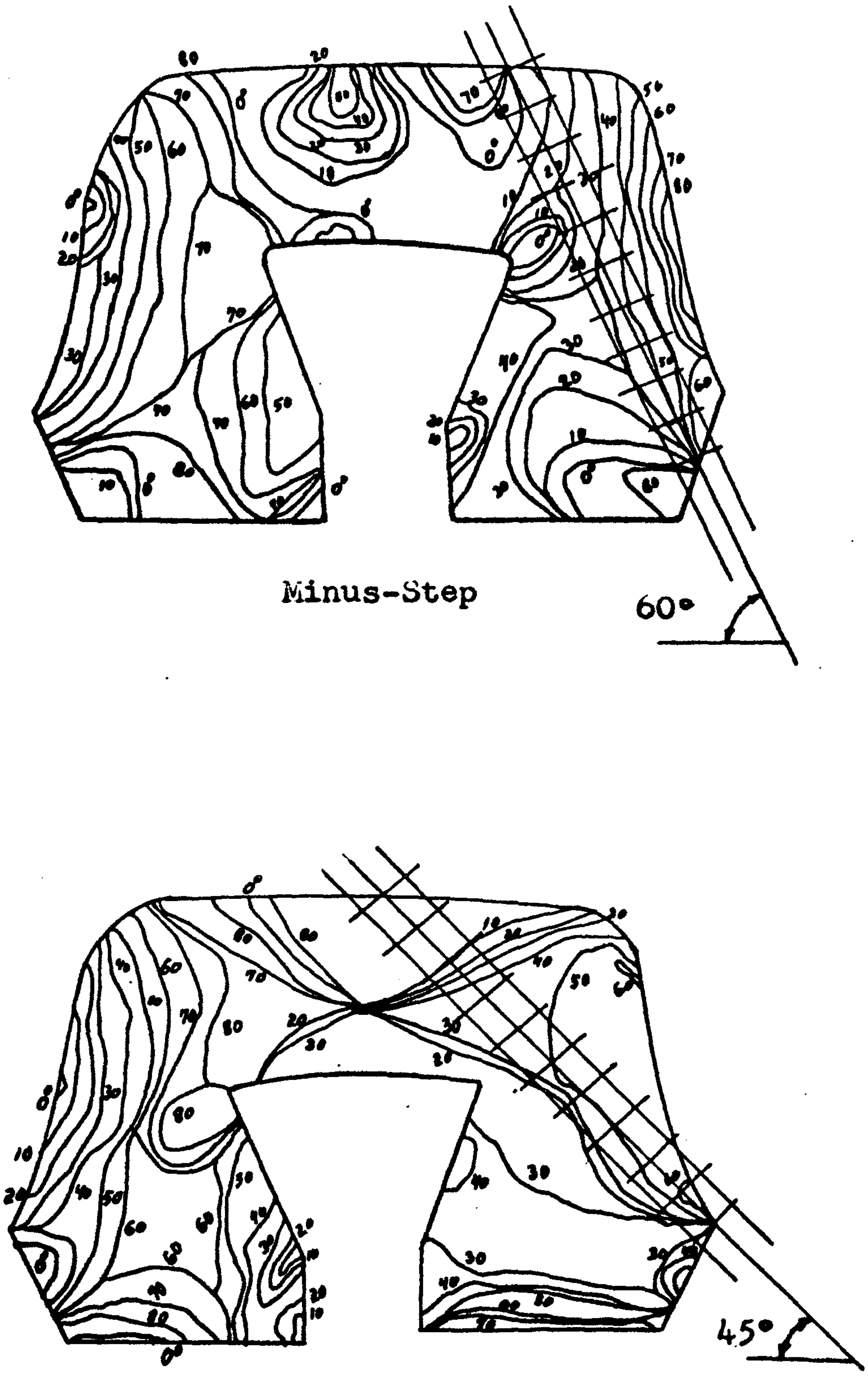

Figure 10. Isoclinic Patterns for Minus-Step and Plus-Step Models

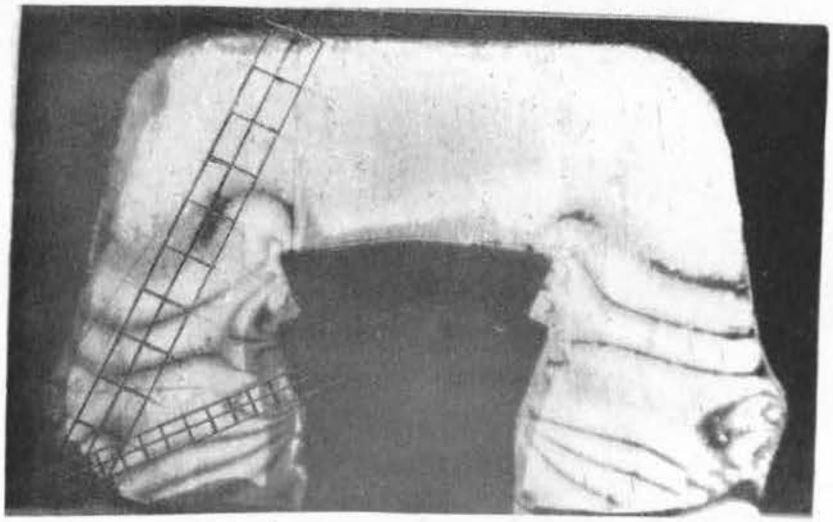

Standard Two-Step Model

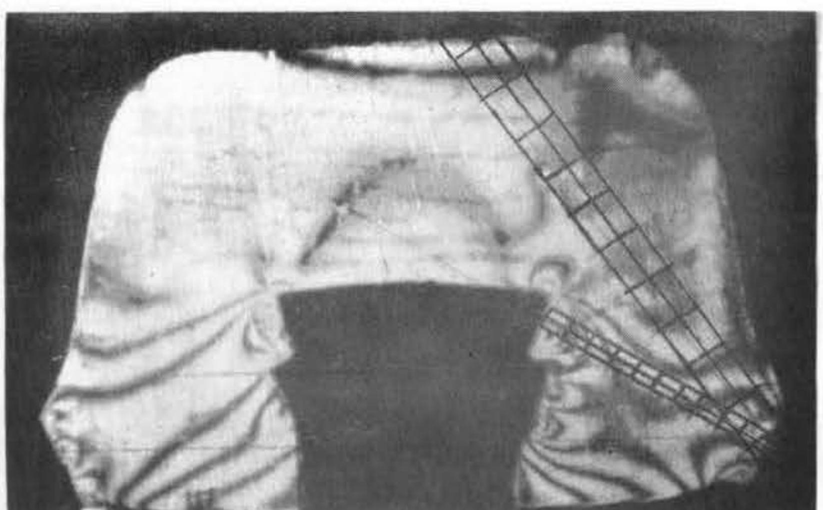

Plus Two-Step Model.

Figure 11. Fringe Patterns for Standard Two-Step and Plus Two-Step Models.

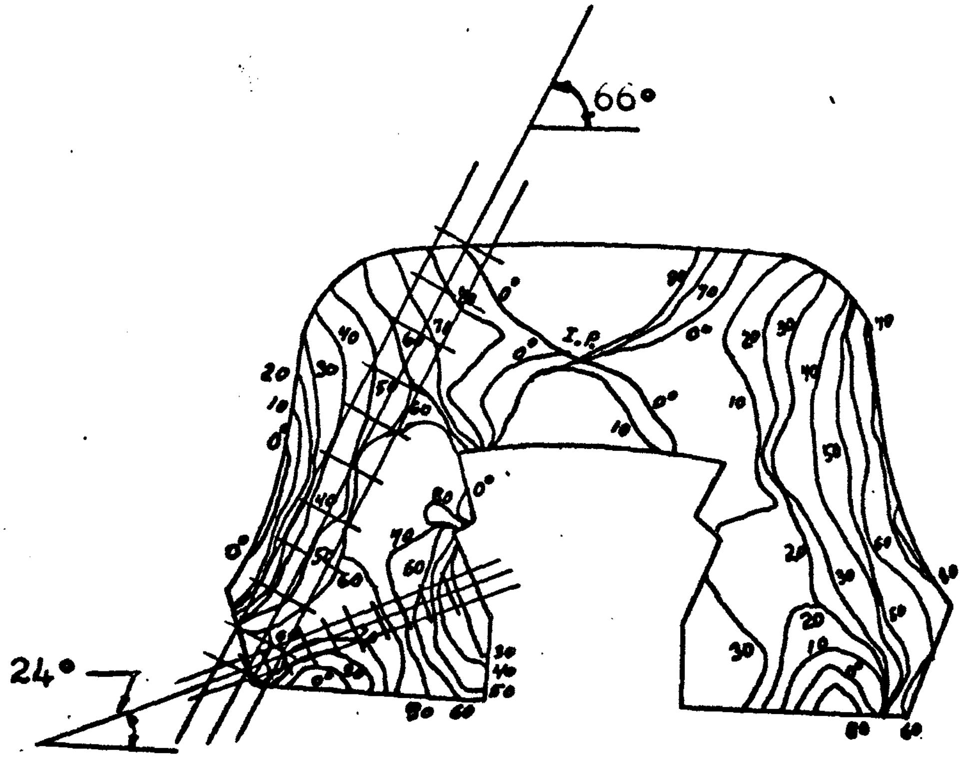

Std.-Two Step

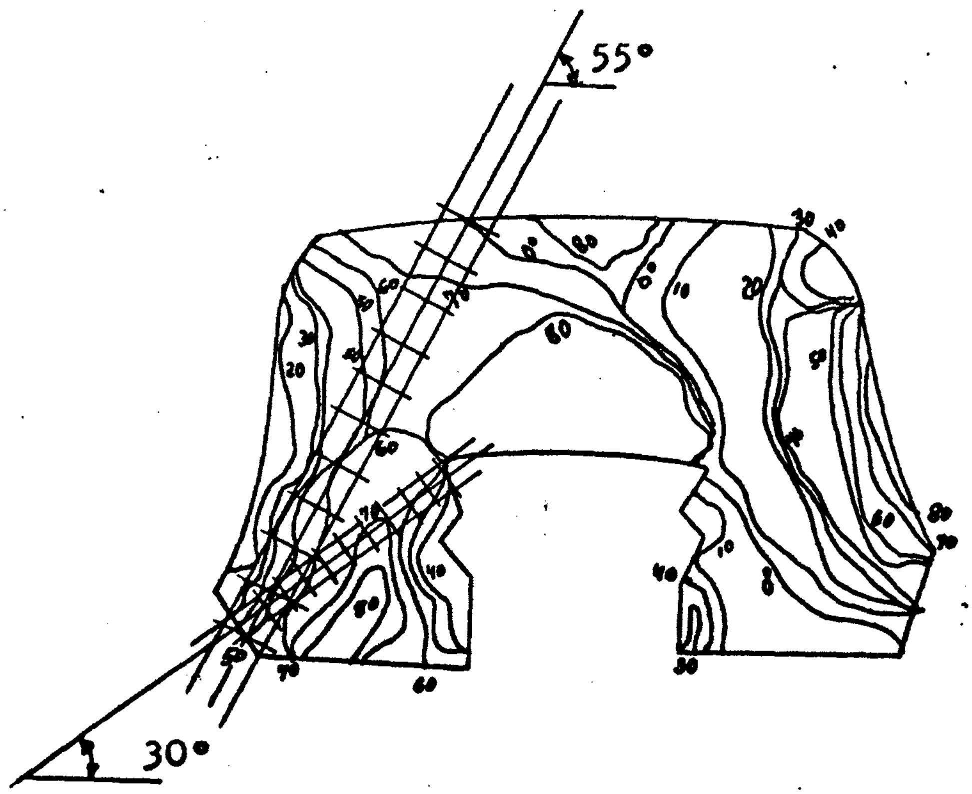

Plus-Two Step

Figure 12. Isoclinic Patterns for Standard Two-Step and Plus Two-Step Models

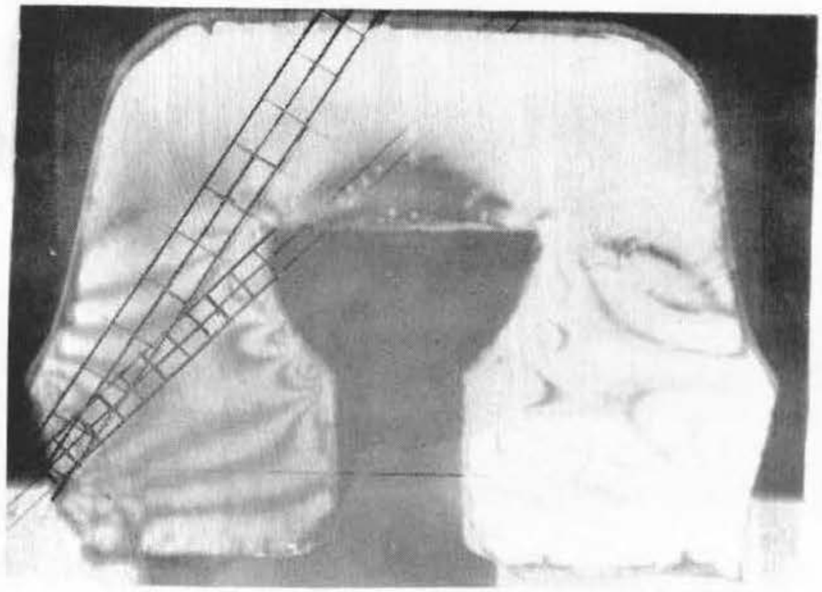

Minus Parabolic Model.

Plus Parabolic Model.

Figure 13. Fringe Patterns for Minus Parabolic and Plus Parabolic Models.

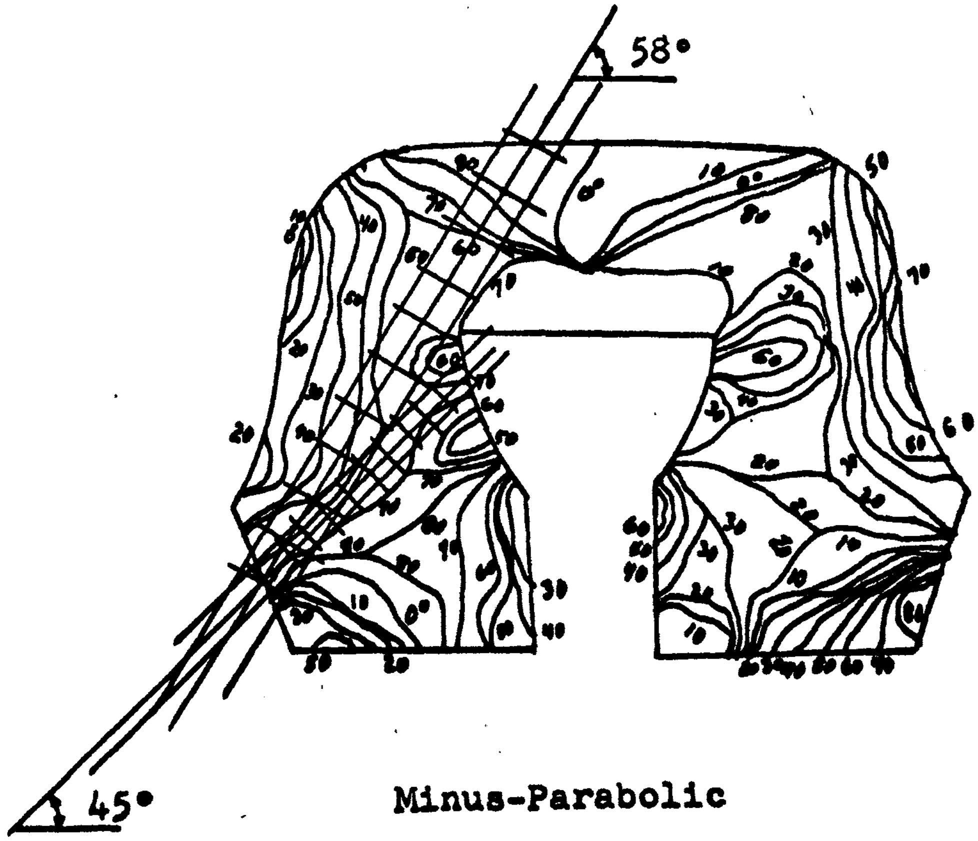

Minus-Parabolic

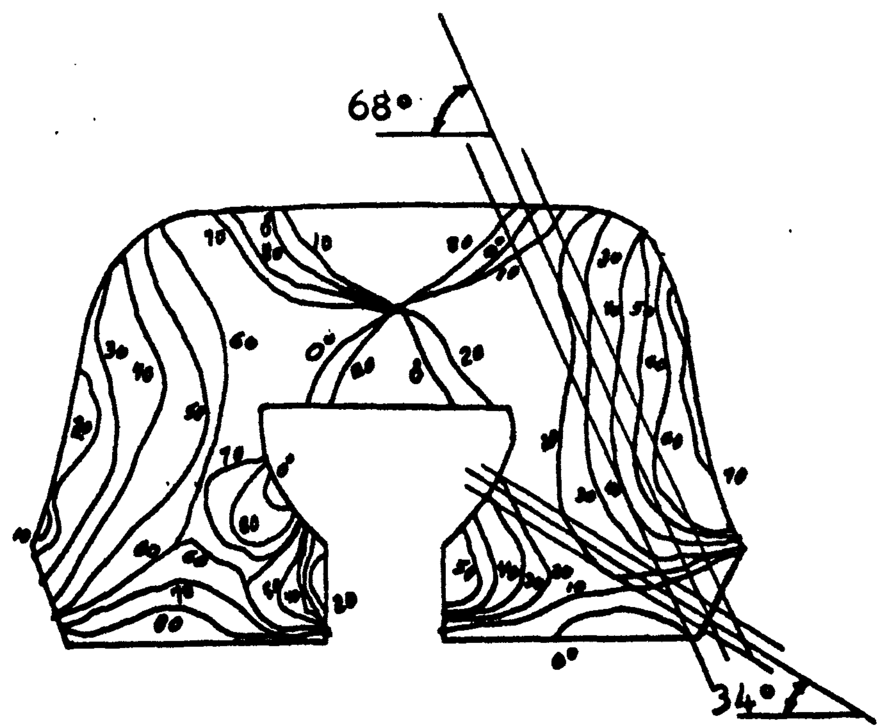

Plus-Parabolic

Figure 14. Isoclinic Patterns for Minus Parabolic and Plus Parabolic Models

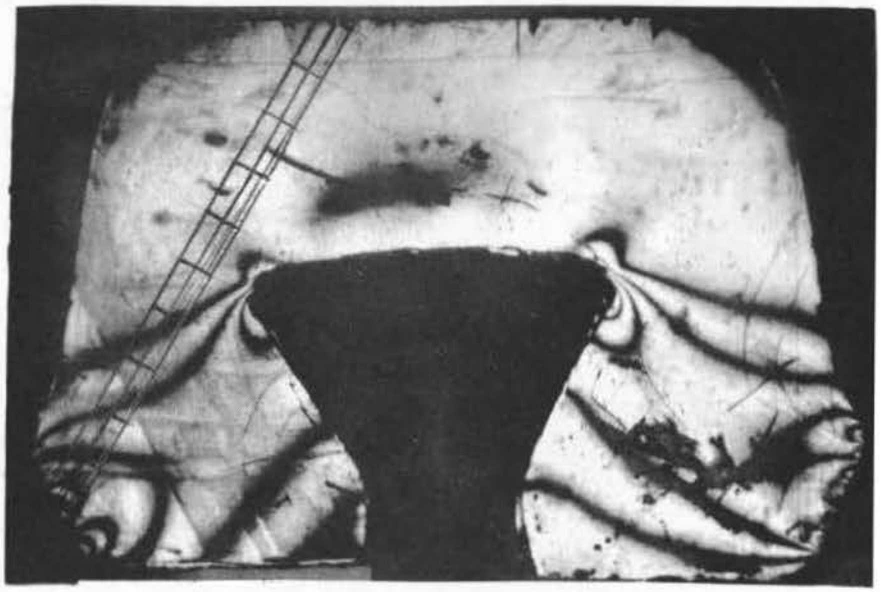

Plus-Plus Step Model.

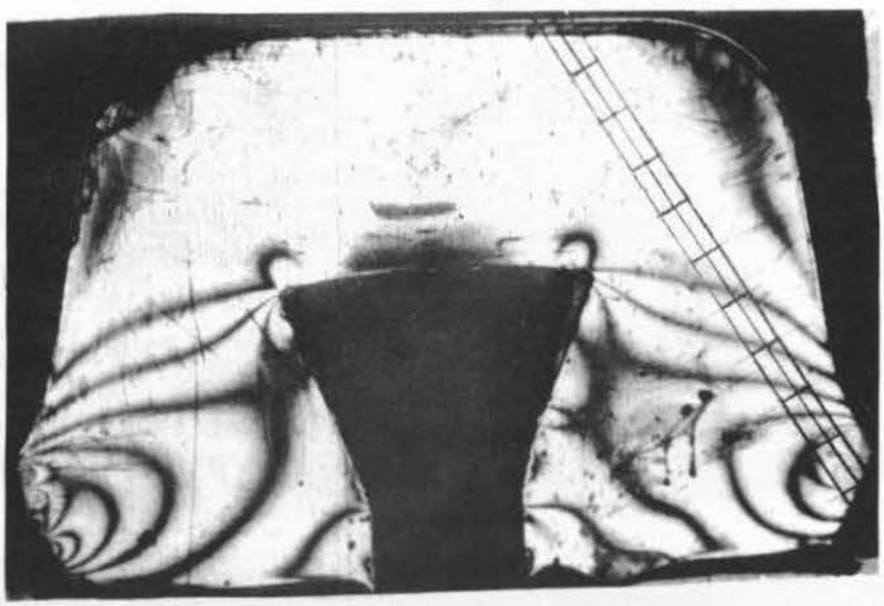

Minus-Minus Step Model.

Figure 15. Fringe Patterns for Plus-Plus Step and Minus-Minus Step Models.

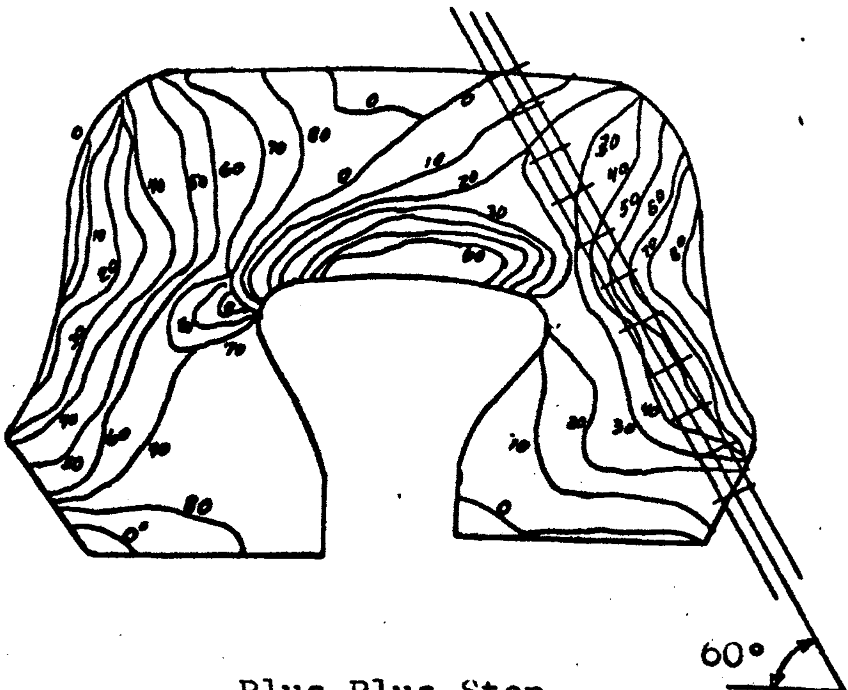

Plus-Plus Step

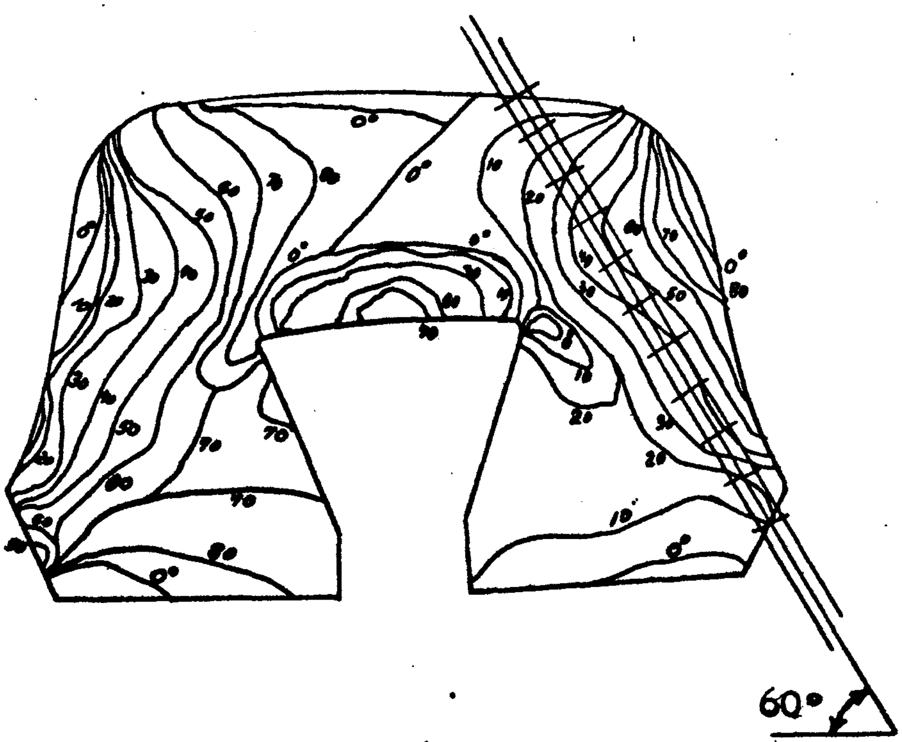

Minus-Minus Step

Figure 16. Isoclinic Patterns for Plus-Plus Step and Minus-Minus Step Models

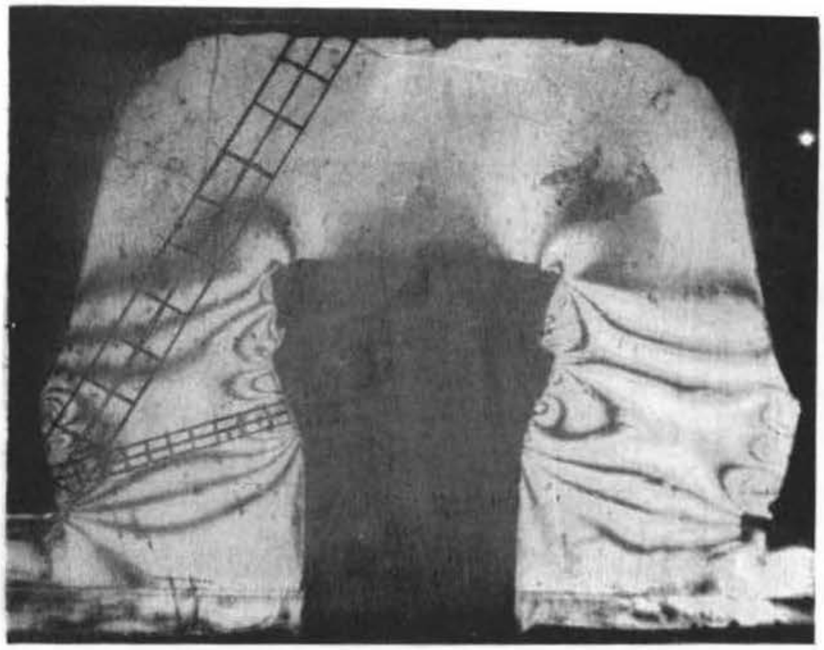

Minus Two-Step Model.

Figure 17. Fringe Pattern for Minus Two-Step Model.

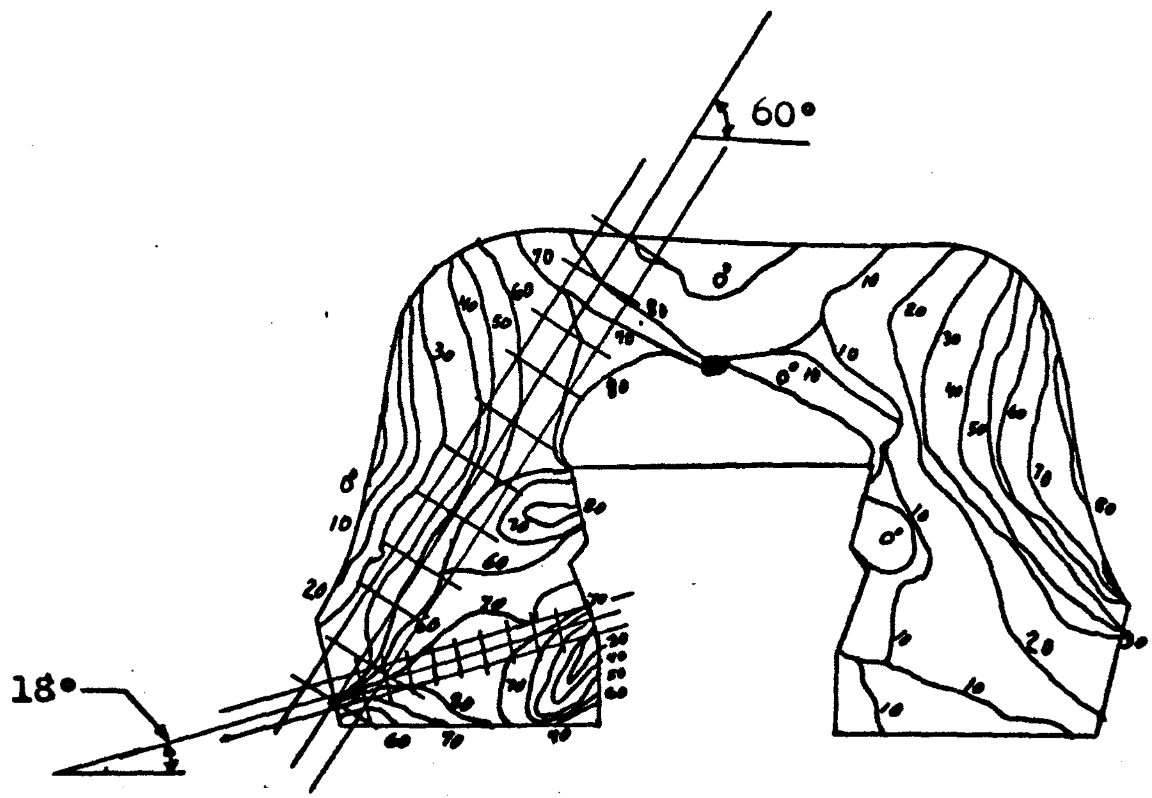

Minus-Two Step

Figure 18. Isoclinic Pattern for Minus Two-Step Model

V. SUMMARY OF RESULTS

Basically two types of data were obtained during these experiments. Photoelastic fringe patterns were obtained at a load of one hundred and eighty pounds on the model and recorded on photographs. Isoclinics, which are loci of points having the same inclination of principal stress, were obtained with a load of one hundred and eighty pounds on the model at angles from 0° to 90° in 10° increments. It was not possible to estimate the accuracy of either the data obtained or the method of computation since no alternate solution to this problem is known. Certain trends and patterns existed in the data obtained that were indicative of a reasonable degree of reliability in the data. It was possible to approximately reproduce the fringe patterns that existed within a model even after a period of several days. No attempt was made to reproduce the fringe pattern after a period of longer than one week. Isoclinic lines normally are difficult to accurately obtain due to breadth of the lines and a fading out of the line near a boundary. The isoclinic parameters obtained during this investigation were in general sharp and distinct even as the line approached a boundary. Because of symmetry of the model and load the isoclinic parameters at all points on one half of the model should be complementary angles to the isoclinic parameters at corresponding points on the other half of the model. This was found to be true from the experimental data. It was noted that normally the experimental isoclinic parameters approached the free boundaries at an angle that approximated the parameters of the isoclinic. The preceeding observation should theoretically exist because the only stress at a free boundary is the principal stress tangent to the boundary.

A tabulation of the maximum principal stress and the maximum shear stress calculated for each model can be found in Table II. Due to the fact that the ultimate strength for both cement and porcelain is much less in tension than it is in compression even a relatively small tensile stress within the structure was considered to be important in the evaluation of the model. It was assumed for this general evaluation that the allowable compressive stress was greater than the allowable tensile stress by a factor of ten.[4]

An examination of Table II shows that the Minus head models possess relatively large tensile stresses regardless of the type of pin used. The Plus head models possess large tensile stresses when used with all of the pins except the Plus Step pin where the lip of the head and the bearing surface of the pin are parallel. The Standard head models also produced large tensile stresses for all of the pins except the case where the lip angle of the head and the bearing surface of the pin were parallel.

The Two Step pin produced regions of high tensile stress in all three heads. This was possibly because the pin produced virtually a vertical pull within the model bending the porcelain as the head deformed radially. The Parabolic pin produced very large tensile stresses in both the Plus

TABLE II. Principal Stresses and Maximum Shearing Stress for All Models Tested

MODEL	ALGEBRAIC MAXIMUM NORMAL STRESS	ALGEBRAIC MINIMUM NORMAL STRESS	MAXIMUM SHEARING STRESS (PSI)
Std.-Step	0	2045 PSIC	813
Plus-Plus Step	29 PSIT	2115 PSIC	875
Minus-Minus Step	791 PSIT	1584 PSIC	1188
Plus-Step	1213 PSIT	1437 PSIC	1325
Minus-Step	1406 PSIT	1278 PSIC	1313
Standard-Parabolic	0	3960 PSIC	938
Standard-Two Step	886 PSIT	1522 PSIC	1188
Plus-Parabolic	987 PSIT	2721 PSIC	1188
Plus-Two Step	663 PSIT	2935 PSIC	1375
Minus-Parabolic	1404 PSIT	2491 PSIC	1313
Minus-Two Step	1952 PSIT	495 PSIC	1250

and Minus heads but no tensile stress and an extremely large compressive stress when used with the Standard head. The Step pin produced large tensile stresses in all of the models except, as previously noted, when the lip and pin angles were equal.

From the preceeding discussion if each of the pins and each of the heads are taken individually none of them appear to produce more desirable stress distribution than any of the others. An examination of combinations of heads and pins indicates that the Single Step pin produces a more desirable stress distribution when the bearing surface of the pin is parallel to the lip of the head. It was not possible to accurately determine the optimum angle for the parallel lip and pin but an optimum angle between 22 1/2° and 27 1/2° was indicated. The Minus-Minus Step model with an angle of 17 1/2° produced high tensile stresses and relatively low compressive stresses. The tensile stresses were sufficiently large to produce fracture at a smaller load than either the Standard Step or Plus-Plus Step models. The Standard Step and Plus-Plus Step models have virtually identical stress distributions and it is not possible to select either in preference to the other.

APPENDICES

APPENDIX A

Sample Calculation.

Model: Plus-Plus Step

The shear difference method is an approximate method of solving the relationship $\sigma_{x_1} = \sigma_{x_0} - \int_0^1 \frac{\partial \tau_{xy}}{\partial y} dx$.[2] (See Figure 19.)

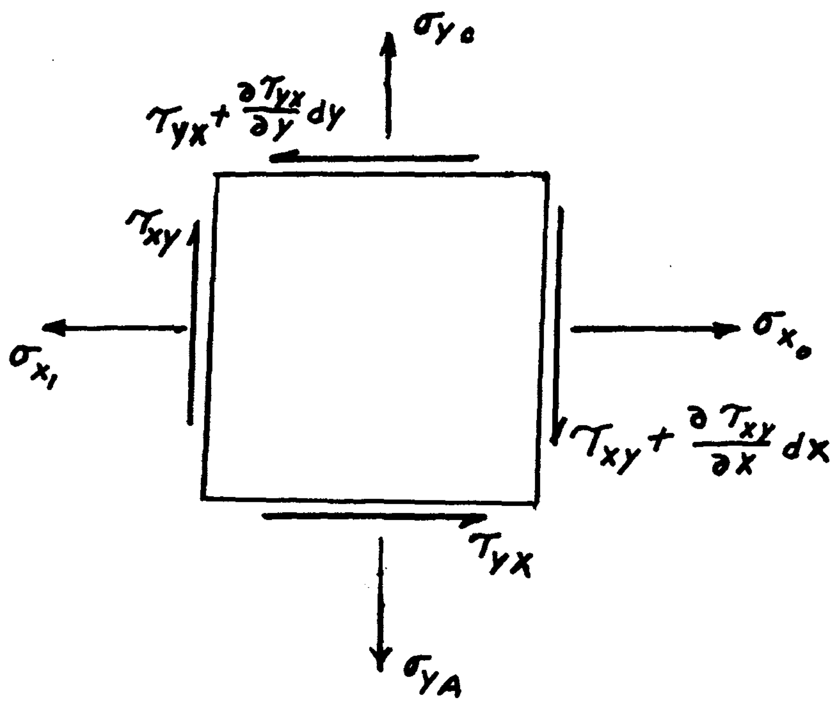

Figure 19. Stress Distribution on a Differential Element.

If the normal stress σ_{x_0} at some point on the X axis is known, and the quantity, $\int_0^1 \frac{\partial \tau_{xy}}{\partial y}$ dx can be approximated by the finite difference in the shearing stress on some finite Y distance then σ_{x_1} can be approximated by converting all horizontal stresses to forces and setting the sum of all horizontal forces equal to zero.

The model was placed in the loading head and a vertical load of 180 pounds was applied to the model through the loading pin. The fringe pattern was photographed. Isoclinic parameters from zero degrees to ninety degrees in ten degree increments were sketched on a sheet of tracing paper. All isoclinic parameters were measured from a horizontal axis. Because of the model deformation the central portion of the top boundary is a stress free boundary. For each model a point was selected where the fringe order and isoclinic parameter were both zero. It can be shown that this is a stress free or singular point in the model. An X axis was constructed from the singular point to the point of greatest fringe order in the model and the Y axis was constructed normal to the X axis with the origin at the singular point. The X axis was divided into ten equal segments, ΔX. (See Figure 20). Two axes parallel to the X axis and equal distances from the X axis were constructed. The shearing stress was calculated on the A axis displaced $+\frac{\Delta X}{2}$ from the X axis and on the C axis displaced $-\frac{\Delta X}{2}$ from the X axis. It was considered desirable to let Y be as small as possible in order to minimize the effect of the slanting of the member at point ten. It was necessary to make Y large enough so that a change in the fringe order and isoclinic parameters on the A, X, and C axes at the points from zero through ten could be detected from the data. The photoelastic data taken consisted of the fringe order (N) and the isoclinic parameter θ.

A rectangle, bounded by the A and C axes and the lines

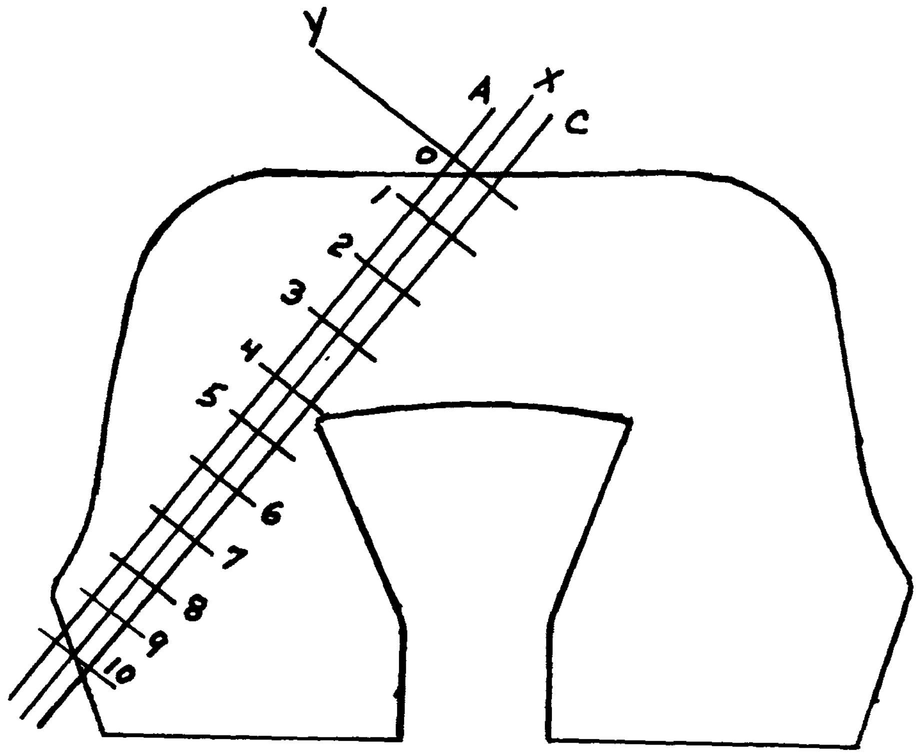

Figure 20. Drawing of a General Model Cross-Section Showing Rectangular Segments Used in the Calculations

parallel to the Y axis through points zero and one, was taken from the body as a free body diagram. A constant thickness was assumed and forces were summed in the X direction. (See Figure 21).

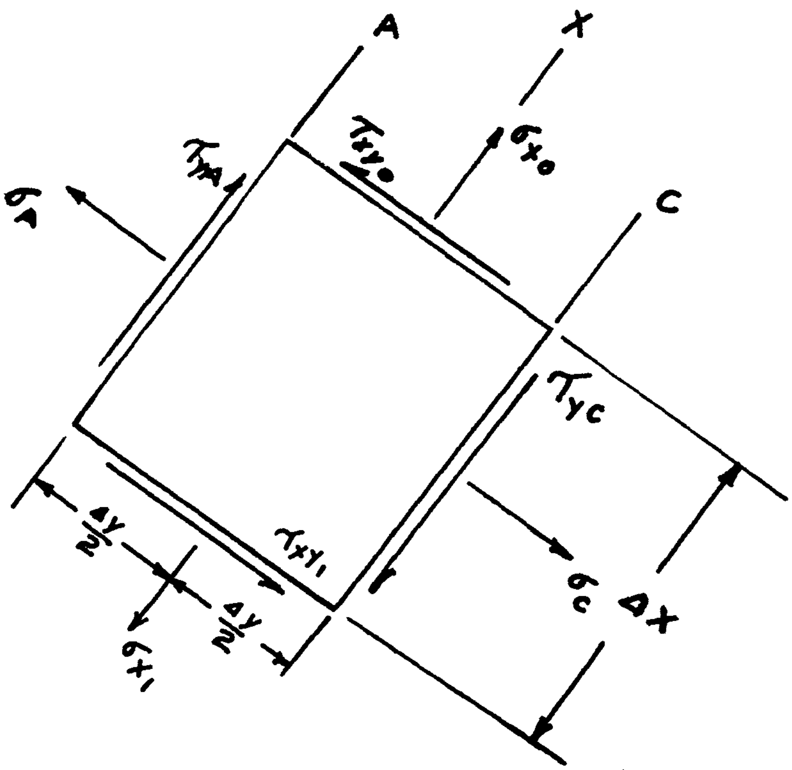

$$\sigma_{X_1} = \sigma_{X_0} - (\tau_{YC} - \tau_{YA}) \frac{\Delta X}{\Delta Y} .$$

Figure 21. Free Body Diagram of a Rectangular Element Extracted From a Model.

τ_{YA} and τ_{YC} are the average shearing stresses on the A and C axes respectively, between points zero and one. It can be seen that the quantity ($\tau_{YC} - \tau_{YA}$) is a numerical approximation of the term $\int_0^1 \frac{\partial \tau_{XY}}{\partial Y} dX$.

The angle Ø was defined as the angle between a plane of principal stress and the X axis and the shearing stress was calculated using the relationship τ_{XY}= NF Sin 2Ø as shown in Table III. The shearing stress was calculated at all points

TABLE III. Shearing Stress Calculations

$\frac{x}{h}$	A-Axis					X-Axis					C-Axis					$\frac{x}{h}$
	η (Fringe)	θ (Deg.)	ϕ (Deg.)	$\sin 2\phi$	τ_{YA} (Fringe)	η (Fringe)	θ (Deg.)	ϕ (Deg.)	$\sin 2\phi$	τ_{YX} (Fringe)	η (Fringe)	θ (Deg.)	ϕ (Deg.)	$\sin 2\phi$	τ_{YC} (Fringe)	
0	--	--	--	--	--	0	0	0	0	0	0	0	0	0	0	0
.1	.30	10	50	.985	.30	.30	11	49	.95	.29	.30	12	48	.961	.29	.1
.2	.50	23	37	.961	.48	.50	22	38	.97	.48	.60	21	39	.977	.57	.2
.3	.50	31	29	.750	.38	.50	29	31	.885	.44	.60	25	35	.940	.56	.3
.4	.70	45	15	.500	.35	.70	30	30	.866	.61	.80	25	35	.940	.75	.4
.5	.70	60	0	0	0	.70	52	8	.276	.19	.90	45	15	.500	.45	.5
.6	.80	60	0	0	0	1.00	50	10	.342	.34	1.00	30	30	.866	.87	.6
.7	1.00	51	9	.309	.309	1.40	47	13	.438	.61	1.60	41	19	.615	.98	.7
.8	1.90	51	9	.309	.59	2.10	45	15	.500	1.05	2.20	41	19	.615	1.35	.8
.9	2.90	40	20	.642	1.86	3.00	31	29	.750	2.25	3.20	29	31	.882	2.82	.9
1.0	5.00	20	40	.985	4.93	7.00	16	44	1.000	7.00	4.50	15	45	1.000	4.50	1.0

Plus-Plus Step Model. Angle between the X-Axis and horizontal is 60°.

from zero to ten for the A, X, and C axes. A graph of shearing stress versus the X displacement from the origin was plotted for the A, X, and C axes as shown in Figure 21. The difference between the shearing stress on the A and C axes was taken from this graph and that difference was also plotted. The quantity $(\tau_{yc} - \tau_{yA})$ was taken as the shearing stress coordinate of the graph of $\Delta\tau$ versus X where X is midway from point zero to point one. The normal stress at point one was calculated using the relationship $\sigma_{x_1} = \sigma_{x_0} - (\tau_{yc} - \tau_{yA})\frac{\Delta x}{\Delta y}$. The stresses were calculated point by point until the normal stresses at point ten were calculated as shown in Table IV. It was imperative to know the direction of the shearing stress on the various axes. This direction was determined by examining a point near the stress concentration at point ten where the maximum stress could reasonably be assumed to be compressive and in a direction approximately normal to the surface of the model at point ten. If the isoclinic parameter is the angle to the plane of algebraic minimum stress at a point the parameters will be the angle to the plane of algebraic minimum stress at all points in the model. It should be noted that the points in the model at which the isoclinic parameter is zero degrees or ninety degrees are points where the parameter changes from being the angle to the plane of one of the principal stresses to being the angle to the plane of the other principal stress. From the basic stress relationships for stresses at a point an expression for the normal stress in the Y direction was

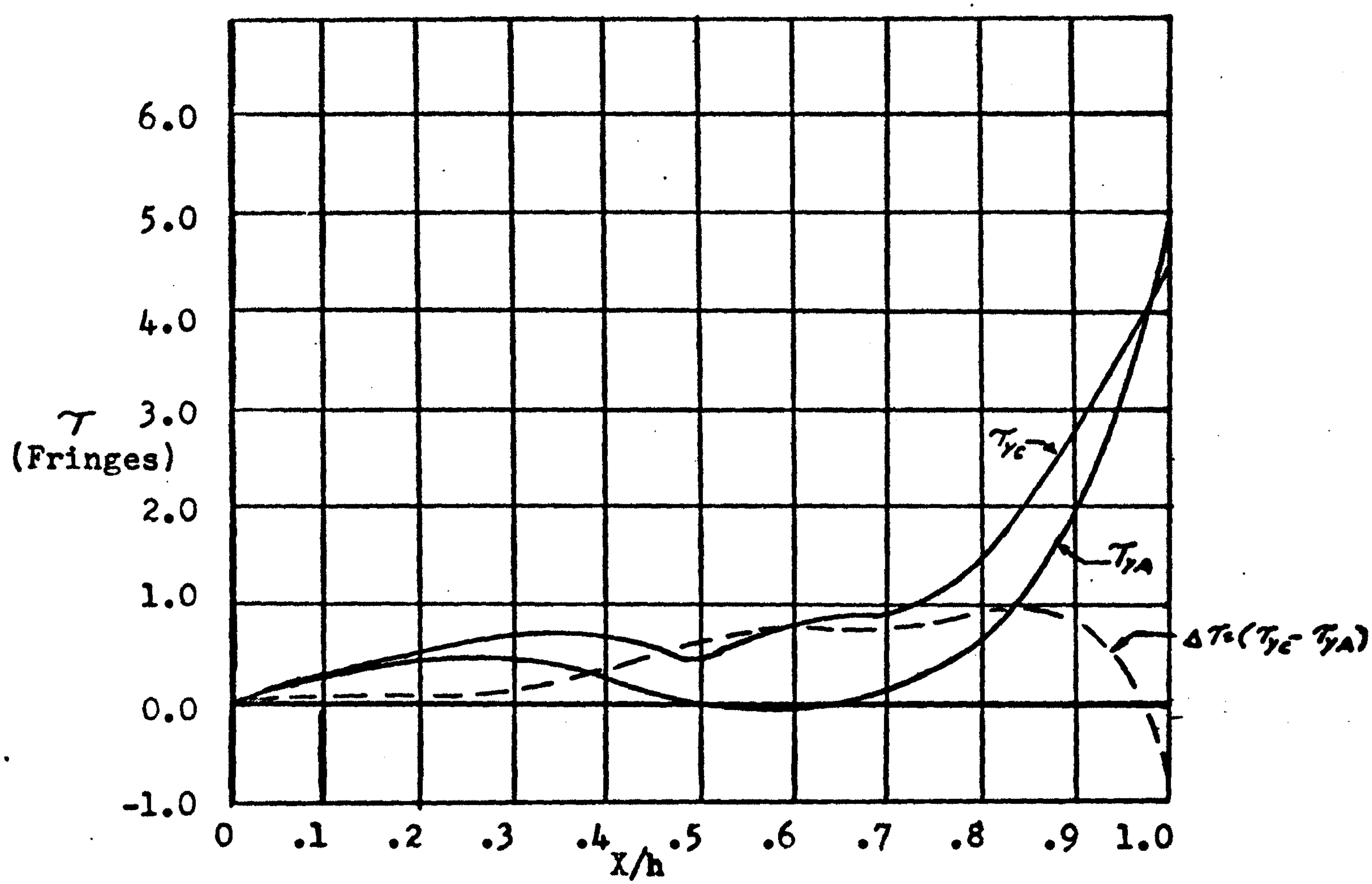

Figure 22. Graph of Shearing Stress Versus Displacement on the X Axis

TABLE IV. Principal Stress Calculations

$\frac{x}{h}$	$\Delta\tau_{xy}\left(\frac{\Delta x}{\Delta y}\right)$ (Fringes)	σ_x (Fringes)	$p-q$ (Fringes)	τ_{xy} (Fringes)	$\sqrt{(p-q)^2-4\tau_{xy}^2}$ (Fringes)	σ_y (Fringes)	σ_x (psi)	σ_y (psi)	$p+q$ (psi)	$p-q$ (psi)	p (psi)	q (psi)	τ_{xy} (psi)
0	0	0	0	0	0	0	0	0	0	0	0	0	0
.1	0	0	.6	.29	.14	- .14	0	- 18	- 18	75	+ 29	- 47	36
.2	.2	- .2	1.0	.48	.28	- .48	- 25	- 60	- 85	125	+ 20	- 105	60
.3	.4	- .6	1.0	.44	.47	- 1.07	- 75	- 139	- 214	125	- 41	- 170	55
.4	.7	-1.3	1.4	.61	.69	- 1.99	- 163	- 249	- 412	175	-113	- 294	76
.5	1.0	-2.3	1.4	.19	1.35	- 3.65	- 288	- 457	- 745	175	-285	- 460	24
.6	1.34	-3.64	2.0	.34	1.88	- 5.52	- 455	- 690	-1145	250	-448	- 697	43
.7	1.64	-5.28	2.8	.61	2.47	- 7.75	- 690	- 968	-1628	350	-639	- 989	76
.8	1.56	-6.84	4.2	1.05	3.64	-10.48	- 858	-1310	-2164	525	-819	-1345	131
.9	1.80	-8.64	6.0	2.25	3.97	-12.61	-1080	-1576	-2656	750	-953	-1703	282
1.0	1.30	-9.94	14.0	7.00	0	- 9.94	-1240	-1240	-2480	1750	-365	-2115	875

$\frac{\Delta x}{\Delta y} = 2.0$ F = 125 psi/fringe obtained. The expression for the normal stress in the Y direction was used in the calculations tabulated in Table IV and is as follows:

$$\sigma_y = \sigma_x - \sqrt{(p-q)^2 - 4\,\tau_{xy}^2}$$

The normal stress in the Y direction was calculated for all points, zero through ten, on the X axis. The principal stresses for each point were then calculated by solving simultaneously the relationships $\sigma_x + \sigma_y = p + q$ and 2N (F) = p-q. (See Table IV).

If the maximum fringe order in the model existed at some point along the contact area between the model and the pin it was not possible to draw a straight line from the stress free point at the top of the model to the point of highest fringe order which was called point twenty. The stress at point twenty was found by following the preceding procedure to find the stresses at point ten. An X' axis was constructed along the line connecting point ten to point twenty. A' and C' axes were constructed using the same procedure that was used in constructing the A and C axes. The basic theory of stresses at a point was used to find the normal stress at point ten in the X' direction. The principal stresses were then calculated for all points between point ten and point twenty using the same procedure that was used to calculate the principal stresses at points zero through ten as shown in Table IV.

APPENDIX B

Following are tabulations of the principal stresses, maximum shearing stress, and the angle to the plane of these stresses measured from a horizontal axis. Point O was omitted from these tabulations because it was in every model a point of zero stress.

TABLE V. Principal Stress and Maximum Shearing Stress for Minus-Minus Step Model

Point No.	p (psi)	θ_p (Degrees)	q (psi)	θ_q (Degrees)	τ_{max} (psi)	θ_τ (Degrees)
1	0	14	- 25	104	13	59
2	23	30	- 76	120	50	75
3	8	45	- 117	135	63	90
4	- 71	50	- 197	140	63	95
5	- 84	42	- 259	132	88	97
6	+ 13	38	- 262	128	138	83
7	+ 84	38	- 416	128	250	83
8	+113	38	- 643	128	388	83
9	+375	21	- 977	111	676	66
10	+791	12	-1584	102	1188	57

θ_p, θ_q, and θ_τ are measured clockwise from the horizontal plane.

TABLE VI. Principal Stress and Maximum Shearing Stress for Plus Plus-Step Model

Point No.	p (psi)	θ_p (Degrees)	q (psi)	θ_q (Degrees)	τ_{max} (psi)	θ_τ (Degrees)
1	+ 29	101	- 47	11	38	56, -34
2	+ 20	112	- 105	22	63	67, -23
3	- 44	119	- 170	29	63	74, -16
4	-118	120	- 294	30	88	75, -15
5	-285	142	- 460	52	88	97, -7
6	-448	140	- 697	50	125	95, 5
7	-639	137	- 989	47	175	92, 2
8	-819	135	-1345	45	263	90, 0
9	-953	121	-1703	31	375	76, -14
10	-365	106	-2115	16	875	61, -29

θ_p, θ_q, and θ_τ are measured clockwise from the horizontal plane.

TABLE VII. Principal Stress and Maximum Shearing Stress for Standard-Step Model

Point No.	p (psi)	θ_p (Degrees)	q (psi)	θ_q (Degrees)	τ_{max} (psi)	θ_τ (Degrees)
1	- 6	167	- 132	77	63	122
2	- 78	152	- 228	62	75	107
3	- 95	150	- 270	60	88	105
4	- 162	150	- 361	60	100	105
5	- 251	147	- 551	57	150	102
6	- 406	152	- 906	62	250	107
7	- 528	144	-1227	54	350	99
8	- 685	144	-1560	54	438	99
9	-1245	150	-2045	60	400	105
10	- 224	120	-1850	30	813	75

θ_p, θ_q, and θ_τ are measured clockwise from the horizontal plane.

TABLE VIII. Principal Stress and Maximum Shearing Stress for Minus-Step Model

Point No.	p (psi)	θ_p (Degrees)	q (psi)	θ_q (Degrees)	τ_{max} (psi)	θ_τ (Degrees)
1	+ 44	3	- 6	93	25	48
2	- 5	12	- 81	102	38	57
3	- 24	20	- 200	110	88	65
4	- 50	22	- 263	112	107	67
5	- 44	31	- 320	121	138	76
6	+ 5	36	- 445	126	225	81
7	+ 52	37	- 598	127	325	82
8	- 79	40	- 955	130	438	85
9	- 112	40	-1278	130	613	85
10	+1406	60	-1221	150	1313	100

θ_p, θ_q, and θ_τ are measured clockwise from the horizontal plane.

TABLE IX. Principal Stress and Maximum Shearing Stress for Plus-Step Model

Point No.	p (psi)	θ_p (Degrees)	q (psi)	θ_q (Degrees)	τ_{max} (psi)	θ_τ (Degrees)
1	+ 12	5	- 38	95	25	50
2	+ 14	10	- 52	100	38	55
3	+ 36	42	- 63	132	50	87
4	+ 88	45	- 88	135	88	90
5	+ 84	49	- 141	139	113	94
6	- 17	50	- 282	140	138	95
7	+ 6	50	- 493	140	250	95
8	- 56	52	- 706	142	325	97
9	- 13	60	-1013	150	500	105
10	+1213	30	-1437	120	1325	75

θ_p, θ_q, and θ_τ are measured clockwise from the horizontal plane.

TABLE X. Principal Stress and Maximum Shearing Stress for Standard-Parabolic Model

Point No.	p (psi)	θ_p (Degrees)	q (psi)	θ_q (Degrees)	τ_{max} (psi)	θ_τ (Degrees)
1	- 7	10	- 56	100	25	55
2	- 33	20	- 133	110	50	65
3	- 68	28	- 244	118	88	73
4	- 104	35	- 338	125	113	80
5	- 168	40	- 418	130	125	85
6	- 232	48	- 557	138	163	93
7	- 304	55	- 779	145	238	100
8	- 399	60	-1125	150	363	105
9	- 541	65	-1640	155	550	110
10	- 502	80	-2370	170	938	125
11	-1255	40	-2705	130	725	85
12	-1890	40	-2890	130	500	85
13	-2150	37	-2950	127	400	82
14	-2225	33	-2975	123	375	78
15	-2272	28	-2998	118	363	73
16	-2315	22	-3015	112	350	67
17	-2390	22	-3090	112	350	67
18	-2495	25	-3245	115	375	70
19	-2523	27	-3497	117	487	72
20	-2460	30	-3960	120	750	75

θ_p, θ_q, and θ_τ are measured clockwise from the horizontal plane.

TABLE XI. Principal Stress and Maximum Shearing Stress for Minus-Parabolic Model

Point No.	p (psi)	θ_p (Degrees)	q (psi)	θ_q (Degrees)	τ_{max} (psi)	θ_τ (Degrees)
1	+ 15	172	- 35	82	25	37
2	+ 76	150	- 50	60	63	15
3	+ 106	145	- 71	55	88	10
4	+ 151	157	- 99	67	125	22
5	+ 335	158	- 265	68	300	23
6	+ 529	145	- 322	55	425	10
7	+ 479	140	- 387	50	525	5
8	+ 353	145	- 947	55	650	10
9	+ 312	150	-1114	60	713	15
10	+ 186	170	-2069	80	1313	35
11	- 188	160	-1937	70	875	25
12	- 264	159	-1640	69	688	24
13	- 21	155	-1396	65	688	20
14	+ 183	153	-1082	63	633	18
15	+ 298	153	- 852	63	575	18
16	+ 316	155	- 760	65	538	20
17	+ 407	160	- 718	70	563	25
18	+ 600	150	- 527	60	563	15
19	+ 986	153	- 490	63	738	18
20	+1404	170	-1223	80	1313	35

θ_p, θ_q, and θ_τ are measured clockwise from the horizontal plane.

TABLE XII. Principal Stress and Maximum Shearing Stress for Plus-Parabolic Model

Point No.	p (psi)	θ_p (Degrees)	q (psi)	θ_q (Degrees)	τ_{max} (psi)	θ_τ (Degrees)
1	+ 10	13	+ 3	103	11	58
2	+ 76	20	- 75	110	75	65
3	+ 115	22	- 134	112	122	67
4	+ 110	31	- 190	121	145	76
5	+ 122	40	- 277	130	166	85
6	+ 59	50	- 366	140	125	95
7	+ 25	55	- 451	145	104	100
8	+ 37	53	- 717	143	187	98
9	- 31	35	- 957	125	+42	80
10	+ 576	10	-1549	100	955	55
11	+ 245	18	-1254	108	750	63
12	- 557	10	-1606	100	525	55
13	- 927	28	-1853	118	463	73
14	-1239	20	-2064	110	413	65
15	-1440	22	-2190	112	375	67
16	-1532	20	-2308	110	388	65
17	-1645	20	-2445	110	400	65
18	-1628	23	-2554	113	463	68
19	-1535	21	-2610	111	538	66
20	- 346	21	-2721	111	1188	66

θ_p, θ_q, and θ_τ are measured clockwise from the horizontal plane.

TABLE XIII. Principal Stress and Maximum Shearing Stress for Standard Two-Step Model

Point No.	p (psi)	θ_p (Degrees)	q (psi)	θ_q (Degrees)	τ_{max} (psi)	θ_τ (Degrees)
1	+ 51	169	+ 25	79	13	34
2	+ 60	157	- 66	67	63	22
3	+117	148	- 83	58	100	13
4	+ 99	145	- 138	55	119	10
5	- 3	150	- 267	60	132	15
6	+ 37	148	- 411	50	225	5
7	- 36	137	- 635	47	300	2
8	-204	140	-1003	50	400	5
9	-417	150	-1416	60	500	15
10	-121	150	-1497	60	688	15
11	-332	150	-1457	60	563	15
12	-355	162	-1330	72	488	27
13	-219	165	-1119	75	450	30
14	- 44	162	- 920	72	438	27
15	+ 23	160	- 802	70	413	25
16	+ 70	152	- 755	62	413	17
17	+183	160	- 791	70	488	25
18	+201	144	- 924	54	563	9
19	+442	100	-1058	10	750	-35
20	+886	90	-1487	0	1188	-45

θ_p, θ_q, and θ_τ are measured clockwise from the horizontal plane.

TABLE XIV. Principal Stress and Maximum Shearing Stress for Minus Two-Step Model

Point No.	p (psi)	θ_p (Degrees)	q (psi)	θ_q (Degrees)	τ_{max} (psi)	θ_τ (Degrees)
1	+ 10	170	- 16	80	13	35
2	+ 45	158	- 54	68	50	23
3	+ 61	155	- 88	65	75	20
4	+ 72	150	- 153	60	113	15
5	+ 8	144	- 218	54	113	9
6	+ 18	140	- 357	50	188	5
7	- 74	142	- 650	52	288	7
8	- 145	140	- 994	50	425	5
9	- 106	136	-1331	46	613	1
10	+1217	130	-1383	40	1250	-5
11	- 447	150	- 960	60	750	15
12	-1559	157	-3124	67	519	22
13	-2070	161	-4140	71	400	26
14	-2310	165	-4620	75	400	30
15	-2335	165	-4695	75	400	30
16	-2330	163	-4660	73	400	28
17	-2270	162	-4540	72	400	27
18	-1710	160	-3470	70	550	25
19	- 531	155	-1083	65	750	20
20	+1952	145	- 887	55	1250	10

θ_p, θ_q, and θ_τ are measured clockwise from the horizontal plane.

TABLE XV. Principal Stress and Maximum Shearing Stress for Plus Two-Step Model

Point No.	p (psi)	θ_p (Degrees)	q (psi)	θ_q (Degrees)	τ_{max} (psi)	θ_τ (Degrees)
1	+ 225	75	- 52	165	138	30
2	+ 369	67	- 32	157	200	22
3	+ 448	61	- 28	151	238	16
4	+ 426	60	- 85	150	250	15
5	+ 325	50	- 351	140	338	5
6	+ 228	60	- 561	150	425	15
7	+ 349	56	- 661	146	500	11
8	+ 269	50	- 957	140	613	5
9	+ 67	50	-1458	140	763	5
10	+ 663	50	-1863	140	1063	5
11	+ 10	50	-1690	140	850	5
12	- 431	57	-2056	147	813	12
13	- 785	60	-2285	150	750	15
14	-1132	65	-2508	155	688	20
15	-1315	68	-2691	158	688	23
16	-1559	74	-2935	164	688	29
17	-1425	70	-2925	160	750	25
18	- 995	60	-2735	150	875	15
19	- 402	54	-2652	144	1125	9
20	+ 539	50	-2211	140	1375	5

θ_p, θ_q, and θ_τ are measured clockwise from the horizontal plane.

BIBLIOGRAPHY

1. Cook, R. D., On a Type of Photoelastic Mottle on an Epoxy Resin, Proceedings of the Society of Experimental Stress Analysis. Volume XXI, Number 1.

2. Frocht, M. M., Photoelasticity, Volume I, 1941, John Wiley and Sons, New York, New York.

3. Polivka, J. J., and Eberhart, H. D., A More Exact Method of Determining Stresses from Photoelastic Isochromatics and Isoclinics, Proceedings of the Fifteenth Semi-Annual Eastern Photoelasticity Conference, June 20, 1942.

4. Salmang, H., Ceramics-Physical and Chemical Fundamentals, translated by Francis, M., London Butterworths, 1961.

VITA

Mr. Richard Lee Pendleton was born in Jefferson City, Missouri on September 4, 1935. He was reared in Owensville, Missouri and received his primary and secondary education in that city. Mr. Pendleton received a Bachelor of Science degree in Mechanical Engineering from Missouri School of Mines and Metallurgy in June, 1957, and subsequently worked for Mobil Oil Company in Oklahoma until August, 1962. From 1962 until the present Mr. Pendleton has been an instructor in the Mechanics Department of the University of Missouri at Rolla.